



Oceanographic and climatic evolution of the Miocene Mediterranean deduced from Nd, Sr, C, and O isotope compositions of marine fossils and sediments

L. Kocsis,¹ T. W. Vennemann,¹ D. Fontignie,² C. Baumgartner,³ A. Montanari,⁴ and B. Jelen⁵

Received 5 September 2007; revised 1 July 2008; accepted 28 July 2008; published 8 November 2008.

[1] Isotopic compositions of marine sediments and fossils have been investigated from northern basins of the Mediterranean to help constrain local oceanographic and climatic changes adjacent to the uplifting Alps. Stable C and O isotope compositions of benthic and planktonic foraminifera from the Umbria-Marche region (UMC) have an offset characteristic for their habitats and the changes in composition mimic global changes, suggesting that the regional conditions of climate and the carbon cycle were controlled by global changes. The radiogenic isotope composition of these fossil assemblages allows recognition of three distinct periods. In the first period, from 25 to 19 Ma, high ϵ_{Nd} values and low $^{87}\text{Sr}/^{86}\text{Sr}$ of sediments and fossils support intense tectonism and volcanism, related to the opening of the western Mediterranean. In the second period, from 19 to 13 Ma the $^{87}\text{Sr}/^{86}\text{Sr}$ ratio of Mediterranean (UMC) deviate from the global ocean, which is compatible with rapid uplift of the hinterland and intense influx of Sr from Mesozoic carbonates of the western Apennines. This local control on the seawater was driven by a humid and warm climate and indicates restricted exchange of water with the global ocean. Generally, the ϵ_{Nd} values of the fossils are very similar to those of Indian Ocean water, with brief periods of a decrease in the ϵ_{Nd} values coinciding with volcanic events and maybe sea level variation at 15.2 Ma. In the third period, from 13 to 10 Ma the fossils have $^{87}\text{Sr}/^{86}\text{Sr}$ similar to those of Miocene seawater while their ϵ_{Nd} values change considerably with time. This indicates fluctuating influence of the Atlantic versus the Paratethys and/or locally evolved seawater in the Mediterranean driven by global sea level changes. Other investigated localities near the Alps and from the ODP 900 site are compatible with this oceanographic interpretation. However, in the late early Miocene, enhanced local control, reflecting erosion of old crustal silicate rocks near the Alps, results in higher $^{87}\text{Sr}/^{86}\text{Sr}$.

Citation: Kocsis, L., T. W. Vennemann, D. Fontignie, C. Baumgartner, A. Montanari, and B. Jelen (2008), Oceanographic and climatic evolution of the Miocene Mediterranean deduced from Nd, Sr, C, and O isotope compositions of marine fossils and sediments, *Paleoceanography*, 23, PA4211, doi:10.1029/2007PA001540.

1. Introduction

[2] Radiogenic and stable isotope compositions of marine sediments and fossils have been documented to be useful proxies for the determination of past oceanic and climatic conditions [e.g., Savin *et al.*, 1985; Zachos *et al.*, 2001; Frank, 2002]. The interpretative strength is particularly good, if different isotopic systems can be used simultaneously.

[3] The application of neodymium isotope geochemistry to oceanography began when it was recognized that the main oceanic provinces have their own characteristic Nd

isotope compositions [Piepgras and Wasserburg, 1980]. The two end-members of the modern seawater are the northern Pacific Ocean and the North Atlantic Deep Water (NADW), which have large differences in their Nd isotopic compositions [e.g., Piepgras and Wasserburg, 1980]. This large variation among the different oceans indicates that neodymium, as well as the other rare earth elements (REE), has a short residence time in seawater relative to the time of global oceanic circulation [e.g., Bertram and Elderfield, 1993; Tachikawa *et al.*, 1999]. Neodymium is mainly derived from atmospheric and riverine terrigenous inputs, while the impact of hydrothermal processes at the mid-oceanic ridges can largely be neglected [e.g., Frank, 2002]. Therefore, differences in Sm/Nd and age for different lithologies of the source rocks in the hinterland can result in differences in the radiogenic isotopic composition of the local seawater. As such, the relatively low $^{143}\text{Nd}/^{144}\text{Nd}$ of the NADW reflects a dominance of erosion of old crystalline rocks of the Canadian Shield, while higher $^{143}\text{Nd}/^{144}\text{Nd}$ of the Pacific Ocean are controlled by a large contribution from erosion of young volcanic rocks. The other ocean basins generally have intermediate $^{143}\text{Nd}/^{144}\text{Nd}$ [Albarède

¹Institut de Minéralogie et Géochimie, University of Lausanne, Lausanne, Switzerland.

²Section des Sciences de la Terre, Département de Minéralogie, University of Geneva, Geneva, Switzerland.

³Institut de Géologie et Paléontologie, University of Lausanne, Lausanne, Switzerland.

⁴Osservatorio Geologico di Coldigioco, Frontale di Apiro, Italy.

⁵Geological Survey of Slovenia, Ljubljana, Slovenia.

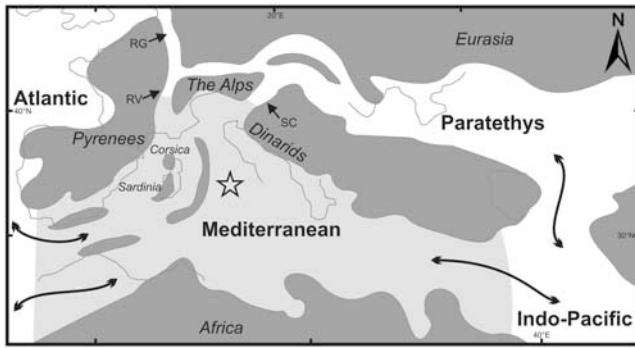


Figure 1. General paleoceanographic situation of the Mediterranean area showing the major oceanic provinces and possible seaways linking this area to the open ocean during the late Oligocene to early Miocene [after Rögl, 1998]. The star indicates the former position of the Umbria-Marche composite sections, and the arrows the possible water currents between the different basins. Other possible gateways marked on the map are RG, Rhine Graben; SC, Slovenian Corridor; and RV, Rhone Valley.

and Goldstein, 1992], related to the pattern of the present global thermohaline circulation and/or related to boundary exchange processes in the shelf areas [Lacan and Jeandel, 2005; Jeandel et al., 2007].

[4] Several archives are used to constrain the ancient oceanic Nd isotope compositions: deepwater Fe-Mn nodules or crusts [e.g., Albarède and Goldstein, 1992; Albarède et al., 1997; Abouchami et al., 1999; Frank et al., 2002], foraminifera [e.g., Palmer and Elderfield, 1985; Vance and Burton, 1999; Burton and Vance, 2000; Pomiès et al., 2002] or fossil fish teeth [e.g., Staudigel et al., 1985; Vennemann and Hegner, 1998; Martin and Haley, 2000]. On the basis of such studies, it was shown that the deepwater of the three main oceanic basins of the Atlantic, Indian, and Pacific were also compositionally distinct during the Oligo-Miocene [e.g., Ling et al., 1997; O’Nions et al., 1998; Burton et al., 1999] and that the Nd isotope compositions of ancient seawater are useful tracers of changes in oceanic circulation, including the opening and closing of gateways to seawater circulation, and/or in estimating continental inputs and mixing of different water masses [e.g., Burton et al., 1997; Frank et al., 1999; Scher and Martin, 2006].

[5] Although some earlier studies have looked at changes in the Mediterranean Nd isotopic compositions [Jacobs et al., 1996a; Stille et al., 1996; Mühlstrasser, 2002], here a more detailed and continuous study on marine deepwater sediments of the Umbria-Marche region in Italy, as well as

of a number of other south Alpine Marine Molasse sediments, were investigated in order to address the variation in the Nd isotope compositions of Miocene seawater in different basins of the Mediterranean during a period of active Alpine-Himalayan tectonism. In addition, deepwater sediment samples from the Ocean Drilling Program (ODP) Site 900 of the eastern North Atlantic close to the Mediterranean outflow were examined to evaluate the importance of the Gibraltar Strait as a gateway between the Mediterranean and the Atlantic Ocean at this time.

[6] To help constrain the effects of local Nd inputs compared to those of the circulating seawater, the neodymium isotopic compositions of calcareous fossils and, where possible, of the carbonate-free bulk sediments containing the fossil were analyzed.

[7] Strontium isotope compositions of marine fossils and sediments were also measured, to help evaluate the effects of local hinterland versus those of the open ocean on the local seawater and hence marine fossil compositions within the Mediterranean basins. Unlike Nd, Sr has a long residence time in seawater, longer than the turnover of the Earth’s oceans, and it was shown that the Sr isotope composition of seawater is similar for the major oceans at any one time [e.g., Burke et al., 1982; DePaolo and Ingram, 1985; Veizer, 1989]. Hence, on the basis of the Sr isotopic composition of well-preserved marine fossils compared to that of the global ocean at the same time, marine sediments may also be indirectly dated [e.g., DePaolo, 1986; Hodell et al., 1991; McArthur et al., 2001].

[8] Finally, oxygen and carbon isotope compositions from benthic and planktonic foraminifera of the Umbria-Marche samples were examined to help evaluate the climatic changes during the Miocene of this part of the Mediterranean and/or to address possible diagenetic changes in isotopic compositions of the fossils used for this study.

2. Geological Setting of the Sampled Sites

2.1. Mediterranean

[9] The Mediterranean Sea today represents the remainder of the most western part of the Mesozoic Neotethys Ocean that vanished by the end of the Eocene because of the Alpine-Himalayan orogeny. During the Miocene, however, the Mediterranean still served as a passage between the Atlantic and Indian Ocean (Figure 1) [e.g., Rögl, 1998]. Several major events changed the shape of the Mediterranean over the course of time (Figure 2a). At the beginning of the Oligocene a new intercontinental sea, the Paratethys, was created to the north of the Mediterranean because of Alpine tectonism. Several seaways opened and closed between the Mediterranean and the Paratethys during the

Figure 2. (a) Geographic and (b) stratigraphic positions of the sampled Miocene marine beds. UMC, Umbria-Marche composite section; MS, Moransengo; VF, Veneto-Friuli area; SLO, Slovenian outcrops; CT, Contessa Valley; MOR, Moria; VED, La Vedova; MDC, Monte dei Corvi Beach; SAR, La Sardella. In the simplified stratigraphic column the numbers correspond to 1, limestone; 2, marly limestone; 3–4, siliceous-calcareous-tuffitic beds; and 5, tuff levels with Raffaello (RAF), Francesca (Franc.), and Respighi (Resp.) levels indicated in the column. See also Tables 1a–1e for further details. The stages and planktonic foraminifera zones are after Gradstein et al. [2004] and Rögl [1998]. The different marks for the sampled layers indicate those where both fossils and sediments (crosses), only fossils (horizontal dashes), or only sediments (vertical dashes) were involved in the isotope measurements.

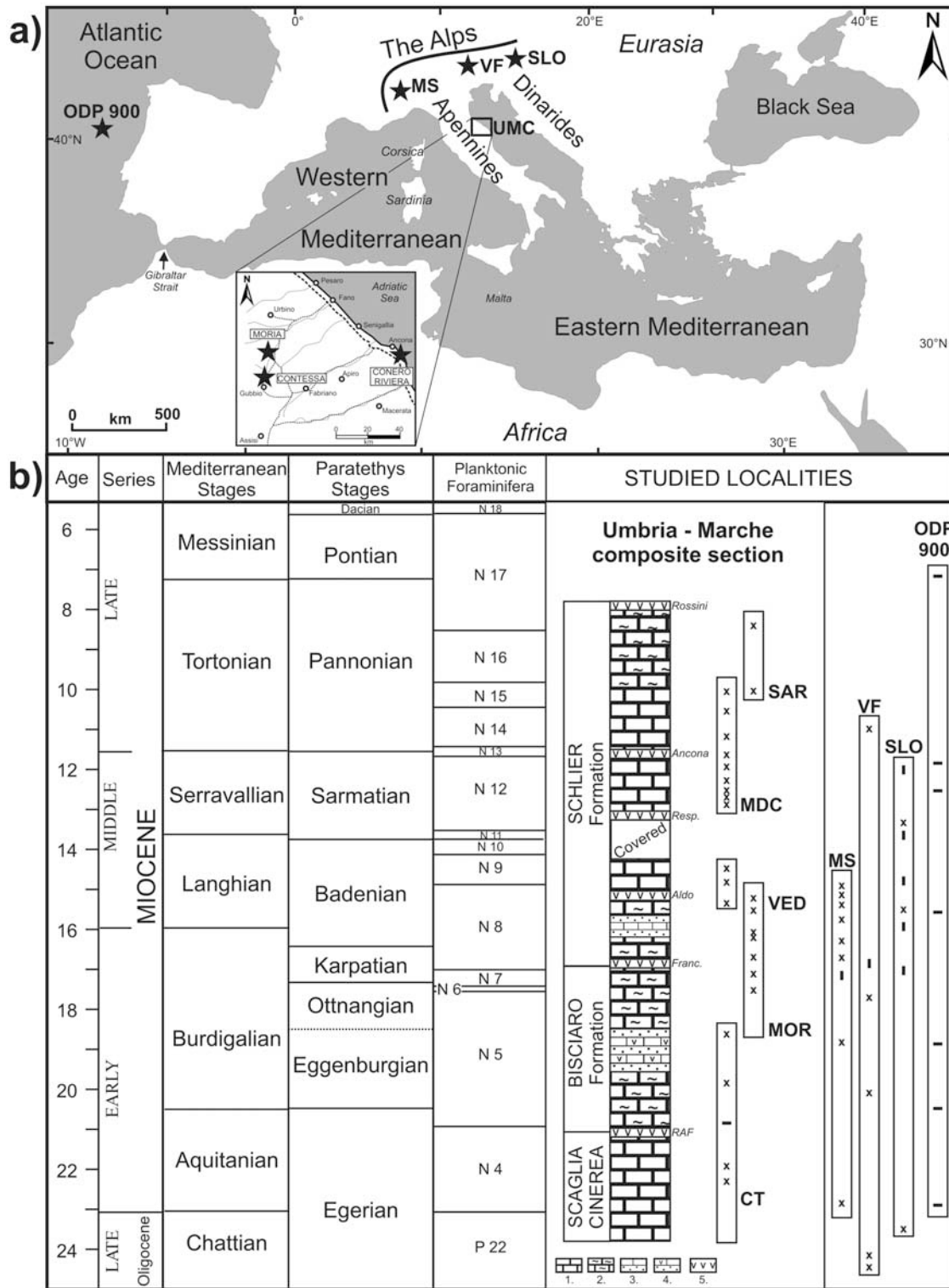


Figure 2

Table 1a. Studied Localities and Layers: Umbria-Marche Composite Section^a

Location	Samples	Meter	Planktonic Foraminifera	Formation	Stages	Absolute Age
Cònero Riviera				<i>Rossini Level</i>		~7.26
Cònero Riviera	SAR+15	206.08	N17	Schlier Formation	Tortonian	8.4
Cònero Riviera	MDC-217	177	N16	Schlier Formation	Tortonian	10.1
Cònero Riviera	SAR-15	176.08	N16	Schlier Formation	Tortonian	10.1
Cònero Riviera	MDC-205	167	N16	Schlier Formation	Tortonian	10.7
Cònero Riviera	MDC-188	156.79	N14-N15	Schlier Formation	Tortonian	11.3
Cònero Riviera		<i>149.85</i>		<i>Ancona Level</i>		~11.68
Cònero Riviera	MDC-154	147.73	N11-N13	Schlier Formation	Serravallian	11.7
Cònero Riviera	MDC-123	137.1	N11-N13	Schlier Formation	Serravallian	12.0
Cònero Riviera	MDC-68	121.13	N11-N13	Schlier Formation	Serravallian	12.4
Cònero Riviera	MDC-42	112.37	N11-N13	Schlier Formation	Serravallian	12.6
Cònero Riviera	MDC-16	104.69	N11-N13	Schlier Formation	Serravallian	12.8
Cònero Riviera	MDC-6	101.36	N11-N13	Schlier Formation	Serravallian	12.9
Cònero Riviera		<i>101.35</i>		<i>Respighi Level (1 cm)</i>		~12.9 ± 0.2
Cònero Riviera	VED-36.2	36.2	N9	Schlier Formation	Langhian	14.6
Cònero Riviera	VED-30	30	N9	Schlier Formation	Langhian	14.8
Cònero Riviera		<i>24</i>		<i>VED-24</i>		~14.9 ± 0.2
Cònero Riviera	VED-17.2	17.2	N8	Schlier Formation	Langhian	15.3
Moria	MOR-184	99	N8	Schlier Formation	Langhian	15.2
Moria		<i>76.8</i>		<i>MOR-76.8</i>		~15.5 ± 0.2
Moria	MOR-155	76	N8	Schlier Formation	Langhian	15.5
Moria	MOR-121	63.8	N8	Schlier Formation	Langhian	16.0
Moria		<i>58.4</i>		<i>MOR-58.4</i>		~16.2 ± 0.2
Moria	MOR-99	57.5	N7	Schlier Formation	? Langhian	16.2
Moria	MOR-59	36	N7	Schlier Formation	Burdigalian	16.7
Moria		<i>19.5</i>		<i>Francesca Level</i>		~17.1 ± 0.2
Moria	MOR-40	18	N7	Bisciaro Formation	Burdigalian	17.1
Moria	MOR-6	3	N6	Bisciaro Formation	Burdigalian	17.5
Contessa valley	CT-62	322.2	N5/6	Bisciaro Formation	Burdigalian	18.0
Contessa valley	CT-51	318.2	N5/6	Bisciaro Formation	Burdigalian	18.6
Contessa valley		<i>311.3</i>		<i>CT-WALL</i>		~19.7 ± 0.3
Contessa valley	CT-28	311	N5/6	Bisciaro Formation	Burdigalian	19.8
Contessa valley	CT-22	309	N5/6	Bisciaro Formation	Aquitanian	20.8
Contessa valley		<i>306.7</i>		<i>RAF</i>		~21.9 ± 0.3
Contessa valley	CT-13	306.5	N4	Scaglia Cinerea	Aquitanian	21.9
Contessa valley	CT-5	303.5	N4	Scaglia Cinerea	Aquitanian	22.3

^aStratigraphic information was obtained from *Deino et al.* [1997], *Montanari et al.* [1997a, 1997b], *Mader et al.* [2001], and *Hilgen et al.* [2005]. Italicized rows represent volcanic ash layers and their obtained ages.

Oligo-Miocene as a result of global sea level changes and orogenesis [e.g., *Rögl and Steininger*, 1983; *Popov et al.*, 2004].

[10] In the late Oligocene, rifting of the Valencia Trough–Gulf of Lion–Ligurian Sea started the formation of the western Mediterranean, also opening many other subbasins during the Miocene [e.g., *Rosenbaum et al.*, 2002]. This was accompanied by short-lived subduction zones, volcanism, and the anticlockwise rotation of Sardinia and Corsica, together with the formation of the Apennine foredeep that shifted east-northeastward [e.g., *Gueguen et al.*, 1998].

[11] In the eastern Mediterranean, the connection with the Indian Ocean remained until the late Burdigalian when the newly formed land bridge between Africa and Eurasia allowed for the migration of terrestrial fauna. Later, the Indo-Pacific seaway reopened, at least twice during the middle Miocene before it finally closed, just shortly after the Langhian/Serravallian transition (~13–14 Ma [e.g., *Popov et al.*, 2004]).

[12] After this time, the Mediterranean had a connection to the global ocean only via the Gibraltar Strait. In the Messinian this gateway was strongly restricted because of major sea level fall that was accompanied by salinity crises in the region. Conditions similar to today were established

by the Pliocene transgression [e.g., *Orszag-Sperber*, 2006; *Popov et al.*, 2006].

[13] To help constrain the oceanic and climatic evolution of the Miocene Mediterranean and to trace the influence of different water masses in the region, a reference section was established. Deep water sediments of the North Apennine foredeep from the Umbria-Marche region in Italy were sampled to construct a composite sequence of Miocene marine sedimentation (Figure 2). The samples were taken from five previously described and well-dated sections that belong to three formations [*Deino et al.*, 1997; *Montanari et al.*, 1997a, 1997b], referred to here as UMC (Umbria-Marche composite section).

[14] The Chattian/Aquitanian boundary (i.e., the Oligocene-Miocene boundary) in the Contessa Valley section (CT), near Gubbio, is in the uppermost part of the Scaglia Cinerea Formation, and bears a hiatus [*Montanari et al.*, 1997a]. The base of the overlying Bisciaro Formation is in the middle Aquitanian (Chron 6AA), and it is marked by a regional bentonite layer (Raffaello Level), which has an Ar/Ar age of 21.9 ± 0.3 Ma [*Montanari et al.*, 1997a]. Samples spanning the Chattian to Burdigalian interval were collected through this CT section, and also in the Moria section (MOR), which is located about 30 km north of Gubbio.

Table 1b. Studied Localities and Layers: Western Monferrato Area^a

Sequence	Samples	Meter	Planktonic Foraminifera	Formation	Stages	Absolute Age
Moransengo	MS-57	620	N8	Tonengo Calcarenites	Langhian	15.2
Moransengo	MS-52	570	N8	Moransengo Sandstone	Langhian	15.4
Moransengo	MS-48	532	N8	Moransengo Sandstone	Langhian	15.5
Moransengo	MS-40	455	N8	Moransengo Sandstone	Langhian	15.8
Moransengo	MS-36	412	N8	Moransengo Sandstone	Langhian	15.9
Moransengo	MS-30	330	N8	Moransengo Sandstone	Langhian	16.2
Moransengo	MS-24	249	base of N7	Moransengo Sandstone	upper Burdigalian	17.2
Moransengo	MS-20	212	N5/6	Antognola Marls	Burdigalian	18.9
Moransengo	MS-7	47	P22	Antognola Marls	upper Oligocene	23.7

^aStratigraphic information was obtained from *Mühlstrasser* [2002].

The Schlier Formation spans from the upper Burdigalian to the Tortonian. Samples covering this time interval have been taken from Moria (MOR) and from three cliff sections along the Cònero Riviera near Ancona, as samples from La Vedova (VED), Mont dei Corvi Beach (MDC) and La Sardella (SAR).

[15] Several volcanoclastic layers occur within these sections and many of them were dated [e.g., *Mader et al.*, 2001]. Given estimates of the sedimentation rates [*Deino et al.*, 1997; *Montanari et al.*, 1997a, 1997b], as well as the biostratigraphic position of the samples, and combining this with recent astronomical and magnetostratigraphic estimates of the ages of the sediments [e.g., *Cleaveland et al.*, 2002; *Hilgen et al.*, 2003, 2005], it was possible to assign absolute numerical ages to the sampled horizons (Table 1a).

[16] Beside the detailed stratigraphy of the area, the paleobathymetry of the basin is not well known. Sediments of the Scaglia Cinerea Formation were deposited in a deep water basin, its pelagic homogenous sequence consisting of well-bedded biomicritic limestone containing sporadic volcanoclastic layers. The older middle Eocene deposits of the Scaglia sequences in the region are deposited in middle-lower bathyal settings (800–1000 m) [*Jovane et al.*, 2007], which might be applicable for the Oligo-Miocene parts as well.

[17] In contrast, the Bisciario Formation is made up of an alternation of different rock types. The lower marly member contains pelagic limestones and calcareous marls, while the middle member is an alternation of siliceous-calcareous-tuffitic beds. The upper member is dominated by marls again, and it is similar to the lower part of the following Schlier Formation. The boundary between these two formations is a volcanoclastic level that can be recognized all over the region (Piero della Francesca Level). The hemipelagic marl of the Schlier Formation is followed by layers

of a calcareous member that is characterized by a rhythmic sequence of foraminiferal, marly limestones grading into marlstones with fewer marly limestone intercalations toward the top. The paleobathymetry was investigated only at La Vedova (VED) section, where an estimate of 600 m was calculated for the Schlier Formation [*Mader et al.*, 2001].

2.2. South Alpine Molasse

[18] Additional samples were taken from the southern Alpine Miocene marine deposits in order to obtain a better spatial distribution of sampling and to help constrain the influence of the terrestrial sediments eroded from the uplifting Alps on the Nd and Sr isotopic composition of the local seawater.

[19] The most western site is the Monferrato (MS) area located east of Turin in northwestern Italy, where the Alps and Apennines are juxtaposed (Figure 2). The area can be subdivided into two main tectonostratigraphic units: Eastern Monferrato that is interpreted as an individual unit, and Western Monferrato that consists of several minor tectonostratigraphic units with well-defined fault-bounded geometric elements [*Clari et al.*, 1995; *Piana and Polino*, 1995]. Samples were obtained from the subunit of Western Monferrato from the Moransengo block (MS) where Chattian-Langhian deepwater (600–1500 m) sediments are exposed (Table 1b) [*Mühlstrasser*, 2002].

[20] The Oligo-Miocene Veneto-Friuli Molasse Basin (VF) is located further east at the junction of three orogenic belts of the Dinarides, Alps, and the Apennine–Southern Alps system. It evolved in two distinct stages. During the Chattian-Langhian, this region was a foreland basin to the Dinarides, formed in response to relatively weak tectonic forces. Nonetheless, four sedimentary megasequences can be distinguished that represent different transgressive-regressive cycles. From the Serravallian onward the tectonic

Table 1c. Studied Localities and Layers: Veneto-Friuli Molasse Basin^a

Sequence	Samples	Sr Age	Location	Stages	Absolute Age
Belluno	Gia-2	16.8	Giazzo	Burdigalian-Langhian	16.8
Belluno	Lib-2	20.1	Libano	lower Burdigalian	20.1
Belluno	Orz-1	24.4	Orzes	Chattian	24.4
Vittorio-Veneto	Lor-2	11.0	S. Lorenzo	upper Serravallian	11.0
Vittorio-Veneto	Zue-1	17.7	Zuel di La	Burdigalian	17.7
Vittorio-Veneto	Nog-1	24.2	Nogaro	Chattian-Aquitian	24.2

^aStratigraphic information was obtained from *Massari et al.* [1986].

Table 1d. Studied Localities and Layers: Slovenia^a

Sequence	Samples	Biostratigraphy	Location	Stages	Absolute Age
B2: Celje basin	L-4-1	NP 25	Petrovè/Lisce	lower Egerian	23.5
B2: Sava folds	ŠJ-25-II-56m		Amon (west of Podèetrtrek)	Sarmatian	12
B2: Sava folds	ŠJ-120-1	Bulimina-Bolivina higher	Mestinje (west of Rog. Slatina)	upper Badenian	13.3
B2: Sava folds	ŠJ-47-2	Bulimina-Bolivina	Mestinje (west of Rog. Slatina)	middle-upper Badenian	13.5
B2: Sava folds	CE-86-1	lower Lagenidae	Kompole (near Štore)	lower Badenian	15.9
A1: Mura basin	Š-58		Šelnica	middle Badenian	14.8
A1: Mura basin	Š-1/a -1	upper Lagenidae	Šentilj (beside the highway)	lower Badenian	15.5
A1: Mura basin	Š-III	lower Lagenidae	Šentilj (beside the highway)	lower Badenian	15.9

^aStratigraphic information was obtained from *Jelen and Rifelj* [2002].

framework changed drastically with extreme subsidence rates and large displacements along the faults, incorporating the basin in the South Alpine–Apennine tectonic system. The basin hence received large amounts of clastic sediments from the Southern Alps [*Massari et al.*, 1986]. Outcrops were sampled near Belluno and in the area of Vittorio-Veneto covering the Chattian-Serravallian (Table 1c), where layers were deposited in a shallow water environment (50–250 m) [*Massari et al.*, 1986].

[21] Further eastward, the Tertiary sediments of Slovenia (SLO) were also sampled, to help trace the connection between the Mediterranean and Paratethys during the Miocene. In this region the rocks are strongly deformed and it is characterized by several faults and broad shear zones [e.g., *Fodor et al.*, 1998]. The present situation results from collision of the Adriatic microplate with the European Plate, involving three large geodynamic systems: the Alps, Dinarides, and IntraCarpathian Basin. At least four different Tertiary tectonostratigraphic units can be distinguished from which two were sampled (A1 and B2, see Table 1d and *Jelen and Rifelj* [2002]).

2.3. ODP Site 900 Eastern North Atlantic

[22] The ODP Site 900 is situated within the Iberian Abyssal Plain west of the Iberia peninsula at 46°40.994'N and 11°36.252'W, where present seawater depth is more than 5000 m. The depositional history of the Iberian Abyssal Plain is characterized by the influence of down-slope transport of terrigenous sediment with various types of debris flow, turbidity current and also contour current reworking [*Milkert et al.*, 1996]. The turbidites may have been triggered by local tectonic activity. At the Site 900 the igneous basement is covered by pelagic-hemipelagic marine deposits with ages from late Paleocene to Pleistocene. However, a hiatus is observed in the late Miocene and the

early Pliocene. The sediments consist mainly of silty, nannofossil claystones and in the younger deposits also of nannofossil chalks. In the older deposits, hemipelagic to pelagic contourite facies with turbidite sediments are dominant, while from the late early Miocene onward, mud-dominated turbidites are common, which decrease up-section giving way to continuous sequences of pelagic marls.

[23] Seven samples were obtained from the ODP East Coast Repository (Table 1e). They were chosen to be time-equivalent to the age of the UMC section in order to determine the ϵ_{Nd} values for the outflow of the Mediterranean. The absolute age of the sampled layers are based on *Milkert et al.* [1996] and *de Kaenel and Villa* [1996].

3. Material and Analytical Methods

[24] All samples were disaggregated with 10% H₂O₂ in an ultrasonic bath; washed with distilled water and sieved (mesh size 125 and 250 μ m). Well-preserved fossils were picked under a binocular microscope. The state of preservation was examined for some samples using a scanning electron microscope (SEM) (Figure 3). The surface of planktonic foraminifera is somewhat etched, but not recrystallized. No oxide coatings were visible for any of the samples. Chamber lumen, apertures and pores can be filled with lithified, carbonate-rich ooze consisting largely of coccoliths. Some early diagenetic dolomite may occur as part of the infill and as overgrowth on the surface of foraminifera. Specimens with visible dolomite were not used for isotope analyses.

[25] For oxygen and carbon isotope measurements benthic and planktonic foraminifera were separated from the UMC section. To test whether species-specific fractionation (vital effect) is preserved or not, different genera (e.g., *Orbulina*, *Globigerinoides*; see Table 2) were measured

Table 1e. Studied Localities and Layers: ODP 900 Eastern North Atlantic^a

Samples	Depth (mbsf)	Planktonic Foraminifera	Calcareous Nannoplankton	Stratigraphic Age	Absolute Ages
149-900-A-14R-4	118.16	N17-N16	NN11	late Miocene	7.1
149-900-A-18R-3	154.91	N11-N9	NN7	middle Miocene	11.9
149-900-A-19R-2	162.65	N8	NN6	middle Miocene	12.5
149-900-A-21R-5	186.63	N7	NN5	middle Miocene	15.6
149-900-A-24R-5	215.93	N6	upper NN2	early Miocene	18.8
149-900-A-27R-5	244.42	N6-N5	NN2	early Miocene	20.4
149-900-A-33R-2	297.88	N4	NN1	early Miocene	22.9

^aStratigraphic information was obtained from *Milkert et al.* [1996] and *de Kaenel and Villa* [1996].

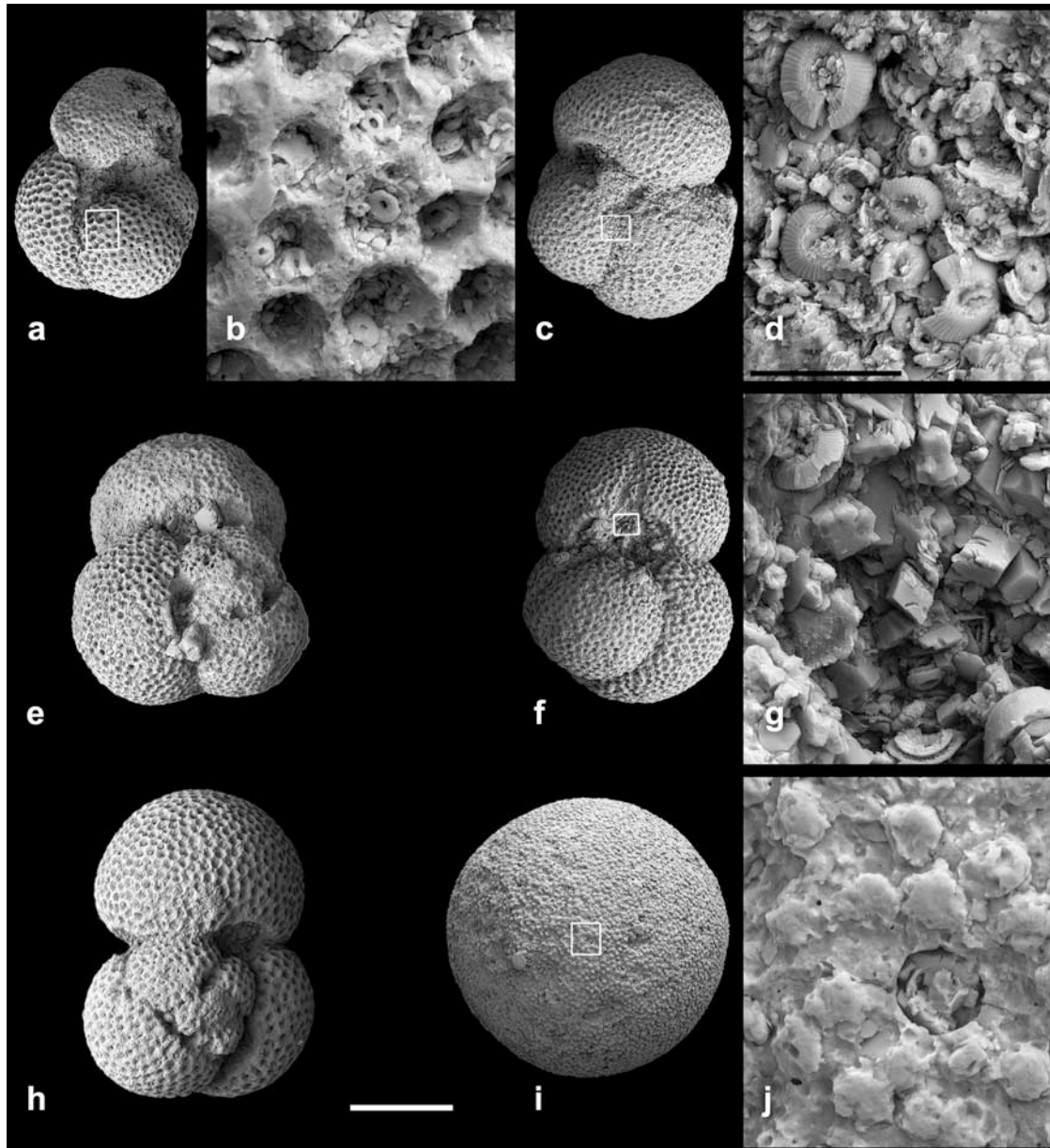


Figure 3. SEM images of planktonic foraminifera of the lineage *Globigerinoides trilobus*-*G. immaturus*-*G. quadrilobatus* (*G. trilobus* s.l. in this paper) from the Umbria-Marche composite sections. For the exact age and position of the samples see Figure 2 and Table 1a. Scale bar at the bottom equals 200 μm . Scale bars of details equal 20 μm . (a) *Globigerinoides quadrilobatus* (d'Orbigny). (b) Detail showing moderately etched pore frames filled in by coccolith ooze and the typical cancellate ornamental wall (MDC-42, Serravallian). (c) *Globigerinoides quadrilobatus* (d'Orbigny). (d) Detail showing test surface covered with well preserved coccoliths: *Coccolithus pelagicus* (Wallich 1871) Schiller 1930 (MDC-68, Serravallian). (e) *Globigerinoides trilobus sacculifer* (Brady); note dolomite rhombohedra at the test surface (MDC-205, Middle Tortonian). (f) *Globigerinoides trilobus* s.l. (g) Detail showing early diagenetic micritic dolomite mixed with coccolith ooze (VED-30, Langhian). (h) *Globigerinoides trilobus immaturus* Le Roy, (SAR-15, Late Tortonian). (i) *Orbulina universa* d'Orbigny. (j) Detail showing well-preserved pustules and pores (MDC-217, Tortonian).

separately. The $\delta^{18}\text{O}$ and $\delta^{13}\text{C}$ values were obtained using a Gasbench II coupled to a Finnigan MAT Delta Plus XL mass spectrometer [Spötl and Vennemann, 2003]. The analytical precision for this method was better than $\pm 0.1\%$.

[26] Oxygen and carbon isotope compositions are expressed in the δ notation relative to VPDB ($\delta^{18}\text{O} = \left(\frac{{}^{18}\text{O}/{}^{16}\text{O}_{\text{Sample}}}{{}^{18}\text{O}/{}^{16}\text{O}_{\text{VPDB}}} - 1 \right) \times 1000$).

Table 2. Oxygen Isotope Composition of the Different Investigated Foraminifera Groups From the UMC Section^a

Samples	$\delta^{13}\text{C}$ VPDB	$\delta^{18}\text{O}$ VPDB
SAR+15		
<i>Orbulina</i>	1.02	-0.68
<i>Orbulina</i>	0.70	-0.51
<i>G. trilobus</i> s.l.	1.60	-0.57
Average	1.11	-0.59
SD	0.46	0.08
<i>Globorotalia</i> : dextral	0.83	0.05
<i>Globorotalia</i> : sinistral	0.72	-0.18
Average	0.77	-0.06
SD	0.08	0.17
MDC-217		
<i>Orbulina</i>	0.11	-0.95
<i>Orbulina</i>	0.20	-1.07
<i>G. trilobus</i> s.l.	0.03	-0.75
Average	0.11	-0.92
SD	0.08	0.16
<i>Globorotalia</i>	-1.02	-0.17
SAR-15		
<i>Orbulina</i>	0.32	-0.55
<i>Orbulina</i>	0.35	-0.71
<i>Orbulina</i>	0.35	-0.72
<i>G. trilobus</i> s.l.	0.76	-0.62
Average	0.45	-0.65
SD	0.21	0.08
Microbenthic (<i>Rotalidae</i>)	-0.07	0.06
<i>Globorotalia</i>	0.13	-0.20
Average	0.03	-0.07
SD	0.15	0.18
MDC-205		
<i>Orbulina</i>	0.77	-0.86
<i>Orbulina</i>	0.89	-1.26
<i>Orbulina</i>	0.45	-0.81
<i>G. trilobus</i> s.l.	0.61	-0.60
<i>G. trilobus</i> s.l.	0.56	-1.03
<i>G. trilobus</i> s.l.	0.47	-0.63
<i>G. bulloides</i>	0.88	-0.84
<i>Orbulina</i>	0.55	-1.05
<i>G. sp.</i>	0.91	-1.13
Average	0.68	-0.91
SD	0.19	0.22
Benthic	0.27	0.19
Benthic	0.08	-0.60
Average	0.18	-0.20
SD	0.13	0.55
MDC-188		
<i>Orbulina</i>	0.92	-1.29
<i>Orbulina</i> and <i>G. trilobus</i> s.l. mixed	1.23	-1.14
<i>Orbulina</i>	1.25	-1.15
Average	1.13	-1.19
SD	0.19	0.09
Benthic	1.08	-0.13
Benthic	0.73	0.28
Average	0.91	0.07
SD	0.25	0.29
MDC-154		
<i>Orbulina</i>	1.00	-0.93
<i>Orbulina</i>	0.76	-0.96
<i>G. trilobus</i> s.l.	0.46	-0.85
Average	0.74	-0.91
SD	0.27	0.06
Microbenthic (<i>Rotalidae</i>)	0.67	0.06
MDC-123		
<i>Orbulina</i>	1.04	-0.70
<i>G. trilobus</i> s.l.	1.05	-0.83
<i>Orbulina</i>	1.02	-0.94
<i>Globogerina</i>	1.03	-0.45
Average	1.03	-0.73
SD	0.01	0.21
<i>Globorotalia</i>	0.92	0.03
Microbenthic	0.56	-0.37

Table 2. (continued)

Samples	$\delta^{13}\text{C}$ VPDB	$\delta^{18}\text{O}$ VPDB
Average	0.74	-0.17
SD	0.25	0.28
MDC-68		
<i>G. trilobus</i> s.l. and <i>G. sacculifer</i>	1.00	-0.65
<i>Globorotalia</i> and <i>Rotalidae</i>	0.20	0.37
MDC-42		
<i>Orbulina</i>	1.00	-0.91
<i>G. trilobus</i> s.l.	1.28	-1.04
<i>G. trilobus</i> s.l.	1.25	-0.78
<i>G. sacculifer</i>	1.01	-1.03
<i>Orbulina</i>	1.17	-1.06
Plankton	1.06	-0.93
Average	1.13	-0.96
SD	0.12	0.11
Benthic	0.43	0.04
Benthic	0.45	-0.13
Average	0.44	-0.04
SD	0.01	0.12
MDC-16		
<i>Orbulina</i>	1.40	-1.00
<i>Orbulina</i>	1.41	-0.98
<i>Orbulina</i>	1.25	-0.95
Average	1.35	-0.98
SD	0.09	0.03
<i>Globorotalia</i>	1.20	-0.82
<i>Rotalidae</i>	1.15	0.20
Benthic	0.59	-0.16
Benthic	0.99	-0.01
Average	0.98	-0.20
SD	0.28	0.44
MDC-6		
<i>G. trilobus</i> s.l. and planktonic fragments	1.41	-0.81
<i>Globorotalia</i> and microbenthic	1.01	-0.09
VED-36.2		
<i>Orbulina</i>	1.86	-1.30
<i>Orbulina</i>	1.97	-1.48
<i>Orbulina</i>	1.94	-1.38
<i>G. trilobus</i> s.l.	2.10	-1.26
Average	1.97	-1.36
SD	0.10	0.10
Microbenthic	1.52	-0.40
VED-30		
<i>G. trilobus</i> s.l.	1.55	-1.52
<i>G. trilobus</i> s.l.	1.55	-1.70
Average	1.55	-1.61
SD	0.00	0.13
<i>Globorotalia</i>	0.98	-0.93
<i>Uvigerina</i>	0.69	-0.42
Microbenthic	0.03	-0.75
Average	0.57	-0.70
SD	0.49	0.25
VED-17.2		
<i>Preorbulina</i> ?	1.65	-2.04
<i>G. trilobus</i> s.l.	1.39	-1.55
<i>G. trilobus</i> s.l.	1.42	-1.44
Average	1.49	-1.68
SD	0.15	0.32
Benthic	0.97	0.15
Benthic	0.48	-0.56
Average	0.73	-0.20
SD	0.35	0.50
MOR-184		
Fragments of globigerinoides	0.92	-2.58
<i>G. trilobus</i> s.l.	1.06	-2.50
Average	0.99	-2.54
SD	0.10	0.06
Fragment of microbenthic	-0.01	-1.96
MOR-155		
<i>G. trilobus</i> s.l.	1.41	-2.13
<i>G. trilobus</i> s.l.	1.54	-2.44

Table 2. (continued)

Samples	$\delta^{13}\text{C}$ VPDB	$\delta^{18}\text{O}$ VPDB
<i>G. trilobus</i> s.l.	1.17	-2.37
Average	1.37	-2.32
SD	0.19	0.16
Benthic	1.12	-1.32
Benthic	1.15	-1.16
Benthic	1.13	-1.69
Average	1.13	-1.39
SD	0.01	0.27
MOR-121		
<i>G. trilobus</i> s.l.	1.08	-2.67
Microbenthic	0.67	-1.46
<i>Rotalidae</i>	0.61	-1.45
Average	0.64	-1.46
SD	0.05	0.01
MOR-99		
<i>Praeorbulina</i>	0.02	-1.73
<i>G. trilobus</i> s.l.	0.96	-2.03
<i>G. trilobus</i> s.l.	0.91	-2.26
<i>G. trilobus</i> s.l.	1.18	-2.36
<i>G. trilobus</i> s.l.	1.00	-1.97
Plankton	0.80	-2.26
Plankton	0.86	-2.14
Average	0.82	-2.11
SD	0.37	0.22
Benthic	1.49	-0.95
Benthic	0.24	-2.24
Benthic	0.13	-1.59
Average	0.62	-1.59
SD	0.75	0.64
MOR-59		
<i>G. trilobus</i> s.l.	0.84	-2.70
Microbenthic (<i>Rotalidae</i>)	-0.31	-1.83
MOR-40		
<i>G. trilobus</i> s.l.	0.42	-3.03
<i>Globorotalia</i>	-0.39	-1.72
MOR-6		
<i>G. trilobus</i> s.l.	0.95	-2.84
<i>Praeorbulina</i>	1.04	-2.51
Average	0.99	-2.68
SD	0.06	0.24
Fragments of microbenthic	1.26	-0.26
CT-28		
<i>G. trilobus</i> s.l.	0.60	-2.71
<i>G. trilobus</i> s.l.	0.48	-2.01
Plankton	0.41	-1.98
Plankton	0.43	-2.66
Average	0.48	-2.34
SD	0.08	0.40
Benthic	0.13	-1.20
CT-13		
<i>G. trilobus</i> s.l.	0.84	-2.81
CT-5		
Planktonic ??	1.62	-2.00

^aBold values indicate average isotopic values for the given layer. These average values are used to plot the data in Figure 4.

[27] For the Sr and Nd isotopic compositions, measurements were made on mixed, well-preserved calcareous fossils because there is no known species-specific fractionation for these isotopic systems. The samples are largely composed of foraminifera, bivalves and in case of some ODP samples, bulk carbonates. An average of about 10 mg of sample (500 mg ODP sediment) was decomposed in 5 molar acetic acid in an ultrasonic bath for 1 h. This method, first proposed by DePaolo and Ingram [1985] was also tested by Hagmaier [2002], where it was confirmed that in contrast to using HCl, no contribution of Sr from the

detrital silicate fraction is leached. The solution was then passed over cation exchange columns for the separation of Nd and Sr [Hegner *et al.*, 1995].

[28] Homogenized, powdered sediment samples were prepared following the method described by Weldeab *et al.* [2002]. Only the carbonate-free, siliceous fraction was analyzed as most of the carbonate within the sediment is either marine in origin and, if present, the older detrital carbonate has very low Nd content compared to that of the siliciclastic detrital component of the sediment [e.g., Faure, 1986].

[29] The isotopic ratios from both sediment and fossils were determined on a Finnigan MAT 262 using a semi-dynamic multiple mass data collection routine. Analysis of NBS-SRM 987 Sr standard yielded $^{87}\text{Sr}/^{86}\text{Sr} = 0.710240 \pm 12$ [2σ , $n = 31$] and the La Jolla Nd standard yielded $^{143}\text{Nd}/^{144}\text{Nd} = 0.511845 \pm 4$ [2σ , external, $n = 26$]. $^{87}\text{Sr}/^{86}\text{Sr}$ are relative to $^{86}\text{Sr}/^{88}\text{Sr} = 0.1194$ and $^{143}\text{Nd}/^{144}\text{Nd}$ to $^{146}\text{Nd}/^{144}\text{Nd} = 0.7219$.

[30] ϵ_{Nd} values are given in Table 3 and are expressed as $\epsilon_{\text{Nd}} = \left[\frac{(^{143}\text{Nd}/^{144}\text{Nd})_{\text{measured}}}{(^{143}\text{Nd}/^{144}\text{Nd})_{\text{CHUR}}} - 1 \right] \times 10^4$, where $^{143}\text{Nd}/^{144}\text{Nd}$ for present-day CHUR is 0.512638 and $^{147}\text{Sm}/^{144}\text{Nd}$ is 0.1967 [Jacobsen and Wasserburg, 1980].

4. Results

4.1. The $\delta^{18}\text{O}$ and $\delta^{13}\text{C}$ Values of Foraminifera From the UMC Section

[31] Oxygen and carbon isotope compositions of the UMC samples are given in Table 2. For some samples, separate analyses of different species were made in order to test the preservation of vital offsets. However, no measurable differences were obtained between compositions of the genera *Orbulina* and *Globigerinoides* (Table 2 and Figure 3). Coccolith ooze present as infill in the foraminifera, while largely having been disaggregated and removed with the ultrasonic treatment, may have influenced the isotopic composition of the foraminifera where residues thereof have remained hidden within the skeletal structure. Averages for planktonic and separately for benthic foraminifera are plotted in Figure 4. A higher standard deviation of the repeated measurements for benthic foraminifera is thought to be the result of a more important and variable influence of the surface-derived coccolith infill in the benthic tests. Despite this, benthic and planktonic foraminifera differ consistently for both C and O isotopes: $\delta^{18}\text{O}$ and $\delta^{13}\text{C}$ values of the planktonic foraminifera are about 0.5 to 1‰ lower and about 0.2 to 0.8‰ higher, respectively, compared to those of the benthic foraminifera.

[32] Between 22.3 to 14.8 Ma the $\delta^{18}\text{O}$ values change from about -3 to -1.5‰ for planktonic and from -2 to -0.2‰ for benthic foraminifera, respectively, while from about 13 Ma the values increase slightly to -1 to -0.5‰ and -0.2 to 0.4‰ for planktonic and benthic foraminifera, respectively.

[33] The carbon isotopic compositions have a general range from -1 to 2‰ with a maximum between 17 to 13 Ma. During this period the trend toward more positive values is more pronounced for the planktonic foraminifera.

Table 3. Sr and Nd Isotopic Compositions of the Studied Sediments and Fossils

Samples	Age	Sediment						Fossils						
		$^{87}\text{Sr}/^{86}\text{Sr}$	2SE ^a	$^{143}\text{Nd}/^{144}\text{Nd}$	2SE ^a	ϵ_{Nd}^0	SD	$^{87}\text{Sr}/^{86}\text{Sr}$	2SE ^a	$^{143}\text{Nd}/^{144}\text{Nd}$	2SE ^a	ϵ_{Nd}^0	SD	
<i>Umbria-Marche Region</i>														
Cònero Riviera	SAR+15	8.4	0.716789	4	0.512112	5	-10.3	0.1	0.709091	16	0.512181	11	-8.9	0.2
Cònero Riviera	MDC-217	10.1	0.715258	7	0.512126	4	-10.0	0.1	0.708807	6	0.512275	24	-7.1	0.5
Cònero Riviera	SAR-15	10.1	0.716692	7	0.512141	5	-9.7	0.1	0.708856	5	0.51223	16	-8.0	0.3
Cònero Riviera	MDC-205	10.7	0.714561	7	0.512093	6	-10.6	0.1	0.708845	8	0.512202	26	-8.5	0.5
Cònero Riviera	MDC-188	11.3	0.714505	63	0.512142	3	-9.7	0.1	0.708831	8	0.51215	13	-9.5	0.3
Cònero Riviera	MDC-154	11.7	0.71503	4	0.512155	3	-9.4	0.1	0.708824	6	0.512127	20	-10.0	0.4
Cònero Riviera	MDC-123	12.0	0.713738	7	0.512126	4	-10.0	0.1	0.708881	6	0.512176	33	-9.0	0.6
Cònero Riviera	MDC-68	12.4	-	-	-	-	-	-	-	-	-	-	-	-
Cònero Riviera	MDC-2	12.6	0.714699	6	0.512149	5	-9.5	0.1	0.708825	5	0.512276	33	-7.1	0.6
Cònero Riviera	MDC-16	12.8	0.714171	10	0.512165	4	-9.2	0.1	0.708819	7	-	-	-	-
Cònero Riviera	MDC-6	12.9	0.716446	8	0.512105	3	-10.4	0.1	0.708849	6	0.512226	24	-8.0	0.5
Cònero Riviera	VED-36.2	14.8	0.708142	9	0.51213	5	-9.9	0.1	0.708700	8	0.512221	10	-8.1	0.2
Cònero Riviera	VED-30	15.0	0.709906	7	0.512123	6	-10.0	0.1	0.708753	6	0.512195	13	-8.6	0.3
Cònero Riviera	VED-17.2	15.3	0.710305	8	0.512172	3	-9.1	0.1	0.708820	8	0.512271	35	-7.2	0.7
Moria	MOR-184	15.2	0.714488	10	0.512124	4	-10.0	0.1	0.708402	8	0.512113	10	-10.2	0.2
Moria	MOR-155	15.5	0.716464	13	0.512124	3	-10.0	0.1	0.708677	9	0.512190	4	-8.7	0.1
Moria	MOR-121	16.0	0.717333	6	0.512127	3	-10.0	0.1	0.708589	8	0.512180	8	-8.9	0.2
Moria	MOR-99	16.2	0.717703	10	0.512120	3	-10.1	0.1	0.708437	7	0.512202	16	-8.5	0.3
Moria	MOR-59	16.7	0.712283	7	0.512126	3	-10.0	0.1	0.708488	5	0.512218	8	-8.2	0.2
Moria	MOR-40	17.1	0.712888	9	0.512105	4	-10.4	0.1	0.708450	6	0.512198	5	-8.6	0.1
Moria	MOR-6	17.5	0.712427	12	0.512126	3	-10.0	0.1	0.708407	7	0.512186	16	-8.8	0.3
Contessa valley	CT-51	18.6	0.711823	6	0.512203	3	-8.5	0.1	0.708272	9	0.512182	28	-8.9	0.5
Contessa valley	CT-28	21.9	0.708976	7	0.512327	3	-6.1	0.1	0.708218	8	0.512334	19	-5.9	0.4
Contessa valley	CT-22	20.8	-	-	-	-	-	-	0.708227	6	0.512385	7	-4.9	0.1
Contessa valley	CT-5	22.3	0.713250	9	0.512199	3	-8.6	0.1	0.708203	6	0.512227	51	-8.0	1.0
<i>Western Monferrato Area</i>														
Moransengo	MS-57	14.9	0.711916	18	0.512175	3	-9.0	0.1	0.708785	9	0.512201	4	-8.5	0.1
Moransengo	MS-52	15.0	0.712942	8	0.512208	5	-8.4	0.1	0.708764	8	0.512157	3	-9.4	0.1
Moransengo	MS-48	15.1	0.712954	10	0.512219	4	-8.2	0.1	0.708824	9	0.512104	7	-10.4	0.1
Moransengo	MS-40	15.2	0.712336	4	0.512151	5	-9.5	0.1	0.708786	8	0.512158	16	-9.4	0.3
Moransengo	MS-36	15.9	0.712033	7	0.512158	4	-9.4	0.1	0.708812	8	0.512104	4	-10.4	0.1
Moransengo	MS-30	16.3	0.713100	8	0.512143	3	-9.7	0.1	0.708766	6	0.512146	9	-9.6	0.2
Moransengo	MS-24	17.2	0.712667	7	0.512167	4	-9.2	0.1	0.708831	12	-	-	-	-
Moransengo	MS-20	18.9	0.714869	11	0.512195	5	-8.6	0.1	0.708604	14	0.512139	5	-9.7	0.1
Moransengo	MS-7	23.7	0.718968	14	0.512152	5	-9.5	0.1	0.708304	17	0.512206	5	-8.4	0.1
<i>Veneto-Friuli Molasse Basin</i>														
Belluno	Gia-2	16.8	0.715627	6	0.512159	8	-9.3	0.2	0.708696	11	-	-	-	-
Belluno	Lib-2	20.1	0.718456	14	0.512105	3	-10.4	0.1	0.708455	7	0.512187	4	-8.8	0.1
Belluno	Orz-1	24.4	0.717382	9	0.512114	4	-10.2	0.1	0.708233	8	0.512345	30	-5.7	0.6
Vittorio-Veneto	Lor-2	11.0	0.712591	7	0.512162	4	-9.3	0.1	0.70886	6	0.512120	34	-10.1	0.7
Vittorio	Zue-1	17.7	0.714277	9	0.512153	4	-9.5	0.1	0.708622	8	0.512201	11	-8.5	0.2
Vittorio	Nog-1	24.2	0.71914	7	0.512201	9	-8.5	0.2	0.708247	6	0.512328	6	-6.0	0.1
<i>Slovenia</i>														
B2: Celje basin	L-4-1	23.5	0.722134	6	0.512157	6	-9.4	0.1	0.708292	8	0.512241	13	-7.7	0.3
B2: Sava folds	ŠJ-25-II-56m	12	0.720543	5	0.512141	32	-9.7	0.6	0.708861	6	-	-	-	-
B2: Sava folds	ŠJ-120-1	13.3	0.716499	9	0.512072	8	-11.0	0.2	0.708851	8	0.512194	19	-8.7	0.4
B2: Sava folds	ŠJ-47-2	13.5	0.711788	5	0.512099	4	-10.5	0.1	0.708848	7	-	-	-	-
B2: Sava folds	CE-86-1	15.9	0.713354	7	0.512137	5	-9.8	0.1	0.709044	8	-	-	-	-
A1: Mura basin	Š-58	14.8	0.723748	10	0.512046	3	-11.5	0.1	-	-	-	-	-	-
A1: Mura basin	Š-I/a-1	15.5	0.718536	6	0.512157	4	-9.4	0.1	0.708846	8	0.512237	14	-7.8	0.3
A1: Mura basin	Š-III	17.0	0.721804	6	0.512114	36	-10.2	0.7	0.709118	16	-	-	-	-
<i>Bulk Carbonate</i>														
Depth (mbsf)	Age	$^{87}\text{Sr}/^{86}\text{Sr}$	2SE ^a	$^{143}\text{Nd}/^{144}\text{Nd}$	2SE ^a	ϵ_{Nd}^0	SD	$^{87}\text{Sr}/^{86}\text{Sr}$	2SE ^a					
<i>Eastern North Atlantic: ODP Site 900</i>														
149-900-A-14R-4	118.16	7.1	0.708822	8	0.512113	5	-10.2	0.1	0.708979	30				
149-900-A-18R-3	154.91	11.9	0.708823	7	0.512138	14	-9.8	0.3	0.708674	13				
149-900-A-19R-2	162.65	12.5	0.708829	10	0.512160	5	-9.3	0.1	0.708849	12				
149-900-A-21R-5	186.63	15.6	0.708705	7	0.512160	4	-9.3	0.1	0.708740	38				
149-900-A-24R-5	215.93	18.8	-	-	0.512185	14	-8.8	0.3	0.708453	31				
149-900-A-27R-5	244.42	20.4	-	-	0.512183	6	-8.9	0.1	0.708315	14				
149-900-A-33R-2	297.88	22.9	-	-	0.512229	6	-8.0	0.1	0.708168	56				

^aInternal uncertainties expressed as two standard errors.

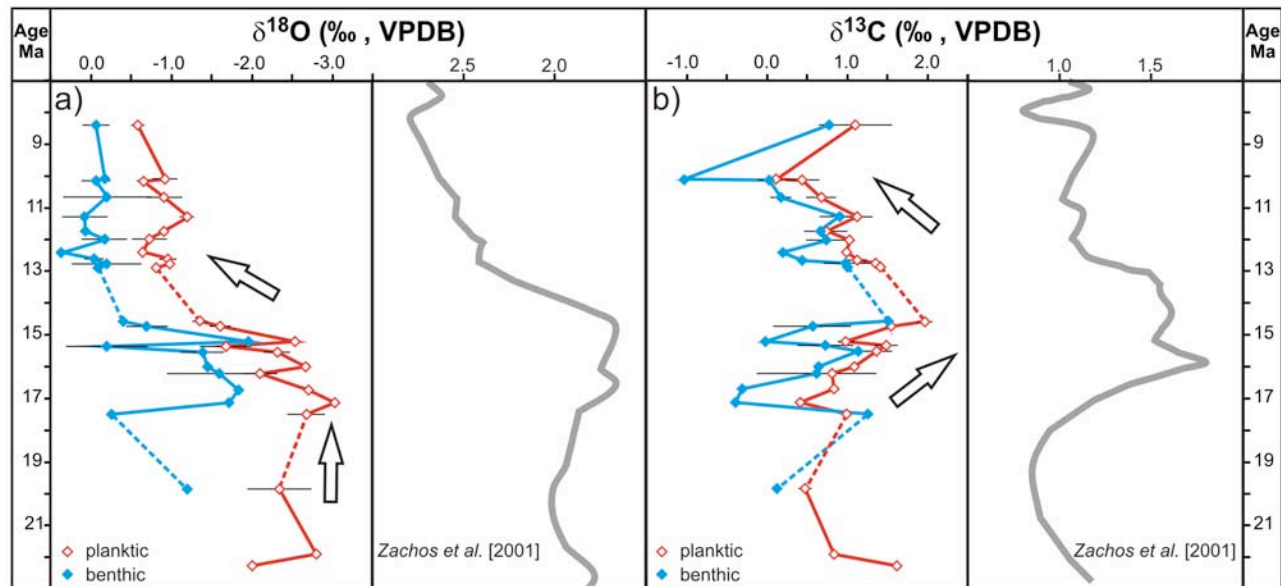


Figure 4. Stable (a) oxygen and (b) carbon isotopic compositions of benthic and planktonic foraminifera from the UMC section and comparison of these values with the mean global isotope record after Zachos *et al.* [2001]. The arrows show the general similarity to the global trends. Note that the scales are different between the two data sets.

4.2. Measurements of $^{143}\text{Nd}/^{144}\text{Nd}$ and $^{87}\text{Sr}/^{86}\text{Sr}$

4.2.1. UMC Section

[34] Nd and Sr isotope compositions are given in Table 3 and illustrated in Figures 5 and 6. The $^{143}\text{Nd}/^{144}\text{Nd}$ of the fossils and sediments vary from 0.512113 to 0.512392 and from 0.512093 to 0.512327, respectively, corresponding to ϵ_{Nd} values of -10.2 to -4.8 and -10.6 to -6.1 , respectively. In general, the values for the sediments are lower or similar to those of the fossils. Samples with an age older than 19 Ma have higher ϵ_{Nd} values for both fossils and sediments compared to those for the rest of the section. After 19 Ma, the sediment ϵ_{Nd} values are quite homogeneous, with an average of -9.9 ± 0.4 , with few exceptions only (e.g., at 15.2 Ma), while the fossil ϵ_{Nd} values cover a wider range with an average of -8.5 ± 0.9 . The fossils have minimum values at 15.2 Ma and around 12–11 Ma, where the ϵ_{Nd} values approach those of the sediment, while three peaks with higher values occur at 15.3, 12.5, and 10 Ma.

[35] The strontium isotope ratios of the fossils have a range from 0.708185 to 0.709091. Samples older than 15 Ma have lower values compared to Miocene open ocean seawater (Figure 5c), while the younger samples have the expected Miocene seawater $^{87}\text{Sr}/^{86}\text{Sr}$, except for the youngest one with a clearly higher $^{87}\text{Sr}/^{86}\text{Sr}$.

[36] The sediment $^{87}\text{Sr}/^{86}\text{Sr}$ vary from 0.708142 to 0.717703 and are generally higher than those of the corresponding fossils, with sample VED-36.2 at 14.6 Ma being the only exception. Other samples from La Vedova (VED) and also samples of CT-13 and CT-28 have much lower $^{87}\text{Sr}/^{86}\text{Sr}$ compared to other sediments and they are also very close to the $^{87}\text{Sr}/^{86}\text{Sr}$ of the fossils.

4.2.2. South Alpine Molasse

[37] The Moransengo fossils have ϵ_{Nd} values from -10.4 to -8.4 and the sediment from -9.7 to -8.2 . Fossils tend to have lower values compared to sediment. However, for the oldest (MS-7) and the youngest (MS-57) samples, the opposite is the case with sediments having lower values, while for yet two other layers (MS-30 and 40) the values are identical between the two archives (Table 3). Mühlstrasser [2002] has already reported Nd data of foraminifera from this area. However, he obtained higher ϵ_{Nd} values, values that are thus also closer to those of the sediments presented here. This discrepancy can be explained by the HCl digestion of the fossils used by Mühlstrasser [2002], which may have leached additional Nd from the detrital components.

[38] The $^{87}\text{Sr}/^{86}\text{Sr}$ ratios have a range from 0.708304 to 0.708831 and from 0.711916 to 0.718968 for fossils and sediments, respectively, with sediment values always higher than those of the fossils. However, the fossils, although having ratios very similar to those of the global ocean $^{87}\text{Sr}/^{86}\text{Sr}$ curve, always have marginally higher ratios during this time interval.

[39] From other studied basins of Veneto-Friuli and Slovenia, six and eight samples were analyzed, respectively. However, the neodymium isotopic ratio in the fossils was not always measurable (Table 3). For samples where this was possible, the fossils have higher ϵ_{Nd} values compared to the sediment, except one sample (Lor-2). The $^{87}\text{Sr}/^{86}\text{Sr}$ ratios of the sediments vary from 0.712591 to 0.719140 and from 0.711788 to 0.723748, respectively. The Sr isotope ages calculated from the $^{87}\text{Sr}/^{86}\text{Sr}$ of the fossils in the Veneto-Friuli Basin are very close to the indicated stratigraphic age [e.g., Massari *et al.*, 1986], with one

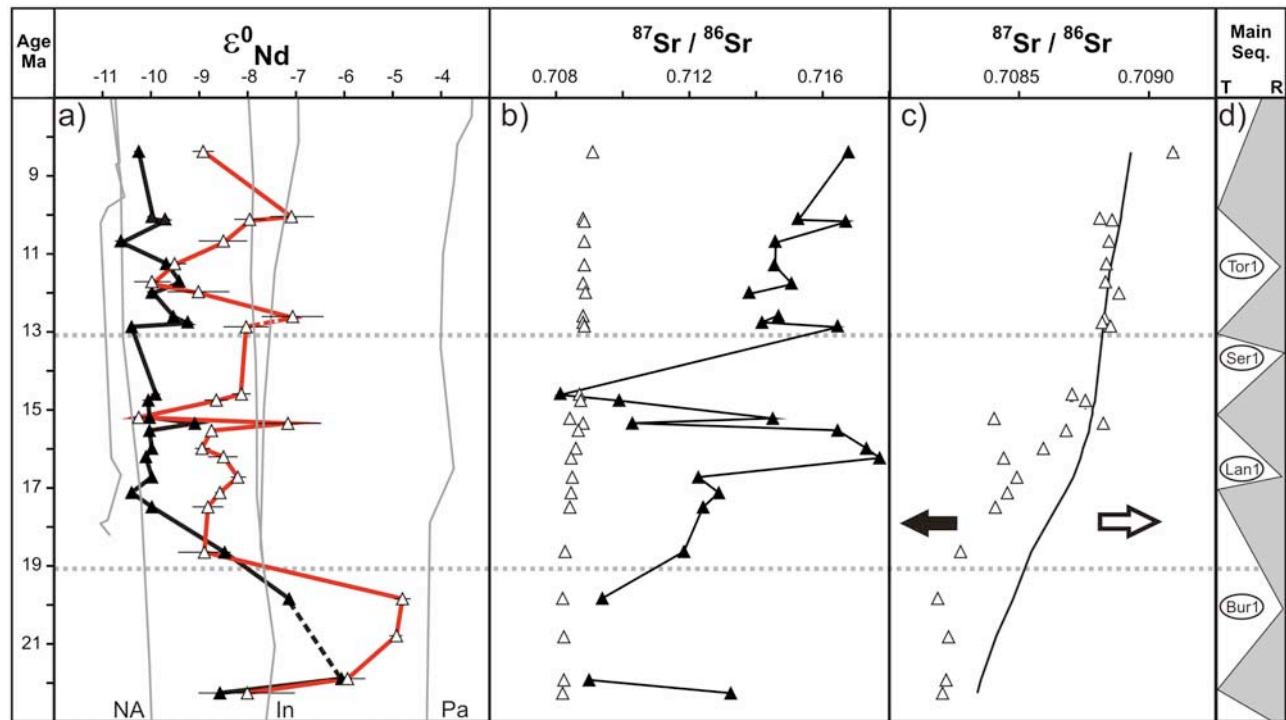


Figure 5. (a) The ϵ_{Nd} values and (b) strontium isotopic compositions of mixed calcareous fossils (open triangles) and the sediment samples (solid triangles) from the UMC section. The reference lines in Figure 5a mark the ϵ_{Nd} evolution of the North Atlantic deepwater (NA) [after *Burton et al.*, 1997; *O’Nions et al.*, 1998]; Indian Ocean (In) [*O’Nions et al.*, 1998], and Pacific Ocean (Pa) [*Ling et al.*, 1997]. (c) Comparison of the $^{87}\text{Sr}/^{86}\text{Sr}$ of the UMC fossils to the Miocene open ocean Sr isotopic composition after *McArthur et al.* [2001]. The open arrow indicates the possible effect of the siliceous detrital components on the fossils [cf. *Gutjhar et al.*, 2007], while the black arrow shows the influence of Mesozoic carbonates on the seawater Sr isotopic composition. (d) Main trends in the eustatic sea level during the studied periods are generalized after *Hardenbol et al.* [1998; see also *Gradstein et al.*, 2004]. T, transgression; R, regression.

exception the Lor-2 sample. These ages were thus used for the plot of Figures 6b and 6c. In case of the Slovenian samples, most of the fossils have higher $^{87}\text{Sr}/^{86}\text{Sr}$ compared to Miocene seawater, given their respective biostratigraphical ages. The oldest sample (L-4) is an exception though.

4.2.3. ODP Site 900

[40] Seven samples were chosen covering the age range of 7–23 Ma (Table 3). Separated foraminifera generally have lower $^{87}\text{Sr}/^{86}\text{Sr}$ and hence would give an older Sr isotope age compared to the indicated biostratigraphical level [*Milkert et al.*, 1996]. Also, for the four youngest samples, $^{87}\text{Sr}/^{86}\text{Sr}$ ratios of bulk carbonates were measured and the values clearly deviate from the corresponding Miocene seawater Sr isotopic composition. Nd isotopic compositions of the samples were analyzed also on the bulk carbonate fractions and the ϵ_{Nd} values gradually decrease from -8 to -10.2 upward with the stratigraphy.

5. Discussion

5.1. Oxygen and Carbon Isotope Compositions of Benthic and Planktonic Foraminifera

[41] Differences expected between the $\delta^{18}\text{O}$ and $\delta^{13}\text{C}$ values of planktonic and benthic foraminifera that have

lived in different habitats within the same water column have been preserved (Figure 4). The lower $\delta^{18}\text{O}$ values of the planktonic foraminifera in this case reflect higher water temperatures near the surface compared to those for the benthic foraminifera of the same age. However, the difference between these average values is generally less than about 1‰, whereas it is over 2‰ for most other open ocean Miocene sections (e.g., *Douglas and Savin* [1975, 1978] for sections from the Central Pacific). Two possibilities could explain this relatively small difference observed for the composite section studied here. For one, the coccolith infill within benthic forams certainly has added a “surface” component to their isotopic value, which is expected to be closer in isotopic composition to that of the planktonic forams. Alternatively, this small difference could also indicate shallower and warmer bottom water conditions with vertical mixing for the Miocene Mediterranean sections studied here compared to the open ocean.

[42] The carbon isotope differences between the two groups do, however, reflect the differences observed for open ocean foraminifera and also for $\delta^{13}\text{C}$ values of dissolved inorganic carbon between the bottom and surface waters [e.g., *Kroopnick*, 1985].

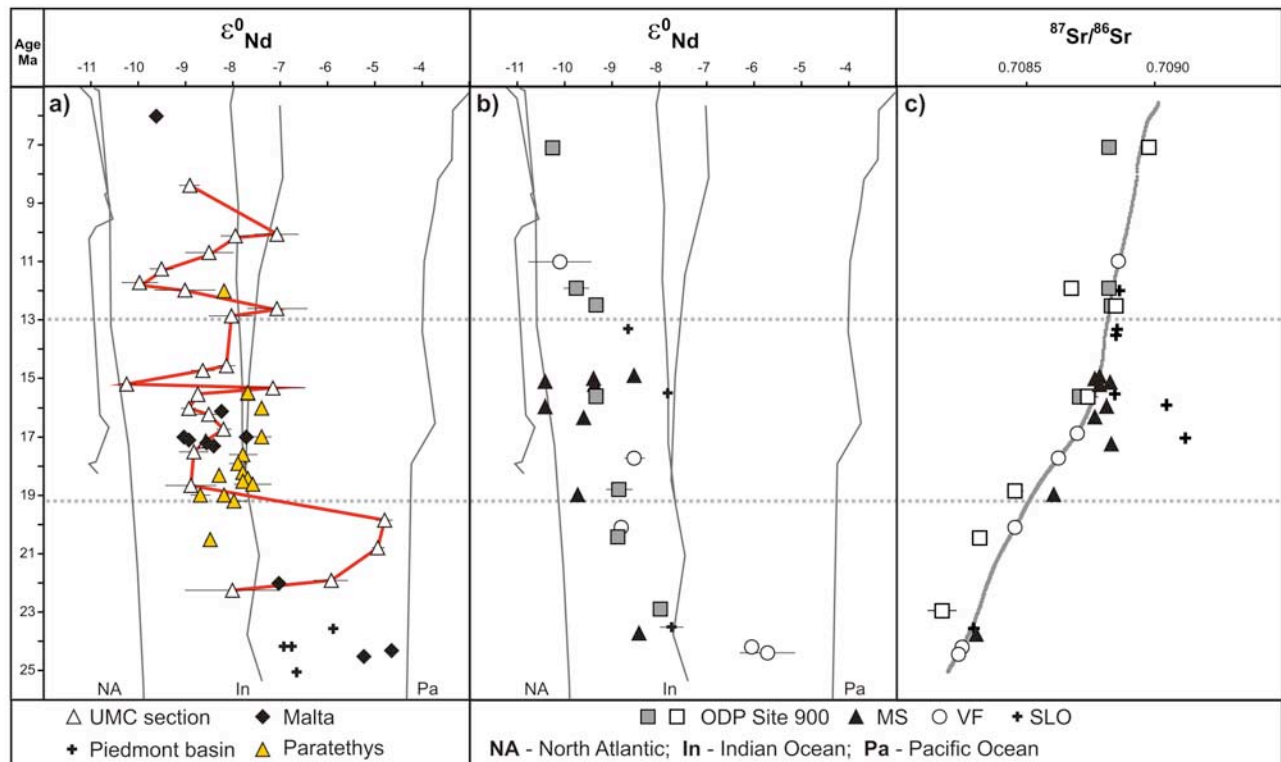


Figure 6. (a) Comparison of ϵ_{Nd} values of the UMC fossils to data from Malta [Stille *et al.*, 1996] (diamonds), Piedmont Basin [Jacobs *et al.*, 1996a] (crosses), and Paratethys [Kocsis *et al.*, 2008] (triangles). (b) The ϵ_{Nd} values and (c) the $^{87}\text{Sr}/^{86}\text{Sr}$ of fossils from the other studied regions: Moransengo, triangles; Veneto-Friuli Basin, circles; Slovenia, crosses; ODP Site 900, gray (bulk sediment) and open (fossils) squares. Note that the general trends in the ϵ_{Nd} values are similar in most of the studied regions. The reference lines in Figures 6a and 6b mark the ϵ_{Nd} values of the North Atlantic deepwater (NA) [Burton *et al.*, 1997; O’Nions *et al.*, 1998], Indian Ocean (In) [O’Nions *et al.*, 1998], and Pacific Ocean (Pa) [Ling *et al.*, 1997], while Figure 6c shows the Miocene open ocean Sr evolution curve [McArthur *et al.*, 2001].

[43] The variations of the carbon and oxygen isotope compositions with time show a similar trend to those of the global oxygen and carbon isotope records (Figure 4), with $\delta^{13}\text{C}$ values also similar in terms of absolute values [e.g., Miller *et al.*, 1987, 1991; Zachos *et al.*, 2001].

[44] The lower $\delta^{18}\text{O}$ values from 22.3 to 14.8 Ma indicate warmer climatic conditions, coinciding with the middle Miocene climatic optimum. The gradual changes to higher $\delta^{18}\text{O}$ values accord well with an onset of global cooling and the development of polar ice sheets [e.g., Zachos *et al.*, 2001].

[45] In terms of $\delta^{13}\text{C}$ values, the positive excursion between 17 and 13 Ma coincides with the globally recognized Monterey event, linking this part of the Mediterranean to the global carbon cycle. This was also observed to be the case for the C isotopic compositions measured for shelf sediments of Malta [Jacobs *et al.*, 1996b].

[46] It can thus be assumed that the fossils analyzed from the UMC section have preserved C and O isotopic compositions characteristic for the habitat and environmental conditions within this basin and the similarity to the global records also supports that this basin has been influenced by

the global changes in climate during the Miocene. This would also argue against a strong diagenetic alteration having affected the chosen samples. Diagenesis, for example, would have led to homogenization of the $\delta^{18}\text{O}$ values. The possible presence of small secondary dolomite that may have remained undetected in some samples (see Figure 3) is thus likely not to have influenced the original isotopic compositions to a large extent.

5.2. Strontium Isotope Composition of the Fossils

[47] Sr substitutes for Ca and is generally incorporated in vivo within biogenic marine carbonate and thus the isotopic composition of the fossils is thought to reflect those of seawater at the time of formation [e.g., DePaolo and Ingram, 1985; Koepnick *et al.*, 1985; Hodell *et al.*, 1991]. However, the $^{87}\text{Sr}/^{86}\text{Sr}$ may also be influenced locally through a strong riverine runoff from the hinterland [e.g., Bryant *et al.*, 1995] and may also be altered during late diagenetic processes. As such, the older samples of the well-dated UMC section with lower strontium isotope ratios compared to Miocene open ocean seawater (Figure 5c), might either reflect a large input of Sr from sources with

low $^{87}\text{Sr}/^{86}\text{Sr}$ [e.g., *Kocsis et al.*, 2007] or reflect alteration in the presence of fluids low in $^{87}\text{Sr}/^{86}\text{Sr}$. Given that the stable C and O isotope compositions appear to be preserved for these fossils, and given that the Sr concentrations in freshwater diagenetic solutions are generally low, Sr input into a marginal sea from a drainage basin with $^{87}\text{Sr}/^{86}\text{Sr}$ lower than that of contemporaneous seawater is considered to be more likely.

[48] The effects of Fe-Mn coatings on the Sr isotopic compositions of the fossils can be an important factor [*Gutjahr et al.*, 2007] as Sr in these phases can be scavenged from the sediment. However, in our case the Sr isotopic compositions of the detrital fraction is generally much higher compared to the fossils (Figure 5c), while the fossils have lower $^{87}\text{Sr}/^{86}\text{Sr}$ compare to the seawater. A source with appropriately low $^{87}\text{Sr}/^{86}\text{Sr}$ could have been the Mesozoic carbonates. According to *Deino et al.* [1997] and *Montanari et al.* [1997a, 1997b], such rocks have discharged sediments from the western Apennines. Indeed, warmer and more humid conditions during the middle Miocene could have also favored weathering of carbonate rocks. Another source of low $^{87}\text{Sr}/^{86}\text{Sr}$ would be the hydrothermal influx from rift zones related to the opening of the western Mediterranean during the early Miocene [e.g., *Gueguen et al.*, 1998]. Contribution of these sources to the Sr budget of the Mediterranean may have been enhanced relative to global seawater as the Gibraltar Strait and/or the eastern Indo-Pacific seaways were also thought to have partially closed several times during the Miocene [*Rögl*, 1998].

[49] The $^{87}\text{Sr}/^{86}\text{Sr}$ between 13 and 9 Ma are similar to those of the global ocean ratios and may reflect that the local control on the Sr budget of the Mediterranean terminated and connections with the global ocean were reestablished. A change toward colder climates during this period may have also decreased the intensity of chemical weathering processes in the hinterland, thus helping to reduce the dissolved Sr input. At 8.4 Ma the youngest sample again deviates from open ocean Sr isotope compositions, indicating yet another closure of the seaways and additional terrestrial influx of Sr.

[50] In case of the sites closer to the Alps, the older fossils appear to reflect the Sr isotopic composition of ancient seawater. However, for samples younger than about 16–15 Ma, the $^{87}\text{Sr}/^{86}\text{Sr}$ in most of the cases deviates toward higher ratios relative to the Miocene open ocean (Table 3). As these localities are close to the tectonically active areas, where older crustal rocks have been exposed (e.g., the Aar and Mont Blanc massifs [*Massari et al.*, 1986; *Kuhlemann et al.*, 2001]), erosion of rocks enriched in ^{87}Sr may again have had an influence on the local seawater Sr budget.

5.3. Neodymium Isotope Composition of the Fossils

[51] Rare Earth Elements (REE) such as Nd are not vital for the formation of biogenic carbonates, nor are they important for the metabolism, hence their content is very low in modern specimens [e.g., *Palmer*, 1985; *Palmer and Elderfield*, 1985]. *Palmer* [1985] argued that most of the REEs in fossil foraminifera are found within Fe-Mn coatings, forming after the death of the organism. Several attempts were performed to remove this coating [e.g., *Boyle*,

1981; *Palmer*, 1985] in order to constrain original seawater or surface water Nd isotopic compositions [e.g., *Vance and Burton*, 1999; *Burton and Vance*, 2000]. In contrast, *Pomiès et al.* [2002] showed that after death of planktonic foraminifera and during subsequent transport through the water column and deposition in the sediment, the primary Nd isotopic composition characteristic of the surface water can be reset, and often the ϵ_{Nd} values of the fossils lie between those characteristic of surface and bottom water. It was also shown that during the cleaning procedure the REEs can readsorb onto the calcite surface [*Pomiès et al.*, 2002]. In contrast, *Vance et al.* [2004] showed that even uncleaned planktonic foraminifera can retain surface water Nd isotope compositions, which can also be retained in the sediment either in the calcite test, Fe-Mn coating or other phases associated with the forams (e.g., organic matter).

[52] Given that mixed benthic and planktonic fossils were measured together, this will give mixed bottom and surface water Nd compositions. However, large differences cannot be expected as the water column was generally well mixed as supported by the oxygen isotope data. Furthermore, the fossils were digested in weak acetic acid, hence assuring that the Nd is largely derived from the calcite lattice, and that additional Nd from incidental Fe-Mn coating is minimized. However, even if contributing to the overall Nd content, such early diagenetic coatings do generally record Nd isotopic compositions of the seawater in which they are formed and thus still allow for interpretations on the seawater geochemistry [e.g., *Palmer and Elderfield*, 1986; *Gutjahr et al.*, 2007]. As Fe-Mn hydroxides are also formed within the sediments they would contribute as a deep water Nd component. Hence, if present, such hydroxides would strengthen the bottom water Nd isotopic composition measured. On the basis of the above arguments [cf. *Frank*, 2002], the ϵ_{Nd} values will be discussed in the context of the overall Nd isotope composition for the Mediterranean.

[53] During the Miocene the three main oceanic basins of the Pacific, Indian, and Atlantic had distinct ϵ_{Nd} values averaging -4 , -8 , and -12 , respectively [*Ling et al.*, 1997; *O'Nions et al.*, 1998; *Burton et al.*, 1999]. The ϵ_{Nd} values of the UMC fossils, during the period from 25 to 19 Ma are between those corresponding to the Indian and Pacific Oceans, while after 19 Ma the values fluctuate between those of the Atlantic and Indian Oceans (Figure 5a).

[54] For the most western localities, such as at Moransengo, some samples have rather low ϵ_{Nd} values in the middle Miocene compared to the other sections, while the Slovenian samples have higher values, that is closer to those corresponding to the Indian Ocean (Figure 6b). The samples analyzed from Veneto-Friuli have values in between these other sites, except for the oldest that have high ϵ_{Nd} values similar to the older UMC samples. The general trend in ϵ_{Nd} values and also the absolute values at the shallow tidal deposits of Veneto-Friuli are remarkably similar to the deeper environments of the UMC sequences indicating good connections and well-mixed water masses between these areas.

[55] The Oligo-Miocene phosphate layers of Malta [*Stille et al.*, 1996] as well as those from upper Oligocene foraminifera from the Piedmont basin [*Jacobs et al.*, 1996a],

by analogy to our study, also show steadily decreasing values from more radiogenic values typical for the Pacific toward lower values typical for the Atlantic Ocean. These data were interpreted to express a gradually decreasing influence of Pacific Ocean and increasing dominance of Atlantic Ocean water in the Mediterranean Sea [Stille *et al.*, 1996]. As the basins within the Mediterranean are commonly relatively small and often represent marginal seas, it is of interest to establish just how much of this overall change can indeed be simply related to changes in oceanographic links and how much of it is related to local hinterland effects only. This question is addressed in the following section.

5.4. Sediment Versus Fossils

[56] Comparing the carbonate free sediment ϵ_{Nd} values to those of the fossils (Figure 5a and Table 3) it is clear that in general these values differ markedly. Given the low Nd content in carbonates of the hinterland, it can be expected that these have not contributed large amounts of Nd to the water column [e.g., Faure, 1986]. In those cases where the ϵ_{Nd} values of the sediment and the fossil are similar, the local Nd input either overwhelmed the Nd budget of the ocean, indicating a more restricted circulation with a more important continental input, or the seawater had a similar Nd isotopic composition compared to the local hinterland input. To address this latter possibility, the exact lithologic constitution and the relief of the hinterland as well as the erosion rates, climatic influence and sea level fluctuations would need to be known. However, the combined use of Sr and Nd isotopes of the sediments as well as the fossils can also be used to address this seawater versus hinterland balance for the control on the seawater geochemical composition.

[57] Mantle-derived rocks and rocks related to young volcanism generally have high ϵ_{Nd} and low $^{87}\text{Sr}/^{86}\text{Sr}$, while old crustal rocks generally have the opposite relationship [e.g., Faure, 1986]. Accordingly, those sediments with high ϵ_{Nd} values but low $^{87}\text{Sr}/^{86}\text{Sr}$ in the older part of the UMC section (Figures 5a and 5b) can be interpreted as being dominated by sediments derived from young volcanic rocks at this time.

[58] This period does coincide with the opening of the western Mediterranean that began around 25 Ma. In addition, the Sardinian and Corsican blocks were subjected to anticlockwise rotation and this was accompanied by increased volcanism in the area [e.g., Gueguen *et al.*, 1998; Rosenbaum *et al.*, 2002]. Volcanic rocks dated at 32 Ma occur in the Provence, France, and large eruptions of rhyodacitic ignimbrites occurred at about 23 to 19 Ma in the Provence, Sardinia, and southern Corsica [e.g., Beccaluva *et al.*, 2004]. Evidence for these eruptions is also given by the volcanoclastic sediments in the Apennine sedimentary sequence, such as the Bisciario Formation in the Umbria-Marche region (26.8–17.1 Ma in the works by Balogh *et al.* [1993] and Montanari *et al.* [1994, 1997a]). Similarly, an effect of volcanism has been detected in the La Vedova region (sample VED-17.2) at 15.3 Ma [Mader *et al.*, 2001].

[59] For the periods where the sediments have higher ϵ_{Nd} values compared to the average values for the section as a

whole, the fossils also have higher values, paralleling the changes in values of the sediments. Hence, this can be interpreted as a direct influence of erosion of the volcanic rocks on the seawater Nd isotopic composition. Similar relations between volcanism and seawater were observed near Iceland [Palmer and Elderfield, 1985] where modern foraminifera also have unusually elevated ϵ_{Nd} values.

[60] Other UMC sediment samples, not having been deposited during periods of known volcanic activity, generally have homogeneous, low ϵ_{Nd} values and high $^{87}\text{Sr}/^{86}\text{Sr}$. This would be compatible with sediment derivation from erosion predominantly of older crustal rocks. The influence of old crustal rocks is also interpreted to have been important for the local seawater Nd isotopic compositions during deposition of the middle Miocene Moransengo fossils, which have very low ϵ_{Nd} values (around -10 , Table 3). Conversely, these low values imply that old crustal rocks were already exposed in the western Alps at this time [cf. Henry *et al.*, 1997; Brügel *et al.*, 2000]. Today the uncovered rocks have a very variable distribution in terms of ϵ_{Nd} values [e.g., Mahlen *et al.*, 2005], however the proportion of eroding old upper continental crust appears to dominate.

5.5. ODP Site 900

[61] Variable Sr isotope compositions from this site are likely to reflect the complex depositional history of the Iberia Abyssal Plain. While largely being characterized by pelagic sedimentation, turbidity flows and reworking by contour currents were common during the early and middle Miocene at this site [Milkert *et al.*, 1996]. The latter processes might have caused some mixing of sediments, which may also account for discrepancies noted for the planktonic foraminifera [Gervais, 1996] and calcareous nannoplankton zonations [de Kaenel and Villa, 1996] relative to the absolute age given by Gradstein *et al.* [2004] (Table 1e and Figure 2b). Nevertheless, oxygen isotope compositions of foraminifera [Mühlstrasser, 2002] are compatible with early to middle Miocene climatic changes.

[62] The ϵ_{Nd} values of fossils (Figure 6a) for this site are surprisingly high compared to those reported for the North Atlantic [e.g., O'Nions *et al.*, 1998; Abouchami *et al.*, 1999; Reynolds *et al.*, 1999]. However, ϵ_{Nd} values higher than those typical for the North Atlantic have also been observed at the Lion Seamount next to the Mediterranean outflow at 7 to 8 Ma [Abouchami *et al.*, 1999]. These higher values were interpreted to result from an additional Nd source from the Mediterranean. As such, the gradually decreasing ϵ_{Nd} values at the ODP Site 900 could indicate a weakening effect of the Mediterranean outflow and strengthening of the North Atlantic deepwater in this area. Conversely, the data also imply that the North Atlantic influence on the Mediterranean could well have become considerably more important from the middle Miocene onward.

5.6. Paleooceanography in the Mediterranean

[63] The combined data set for the O, Sr and Nd isotopic compositions of the fossils, in conjunction with interpretations of paleontological changes given in the literature [e.g., Rögl, 1998] allows for the distinction of three periods for

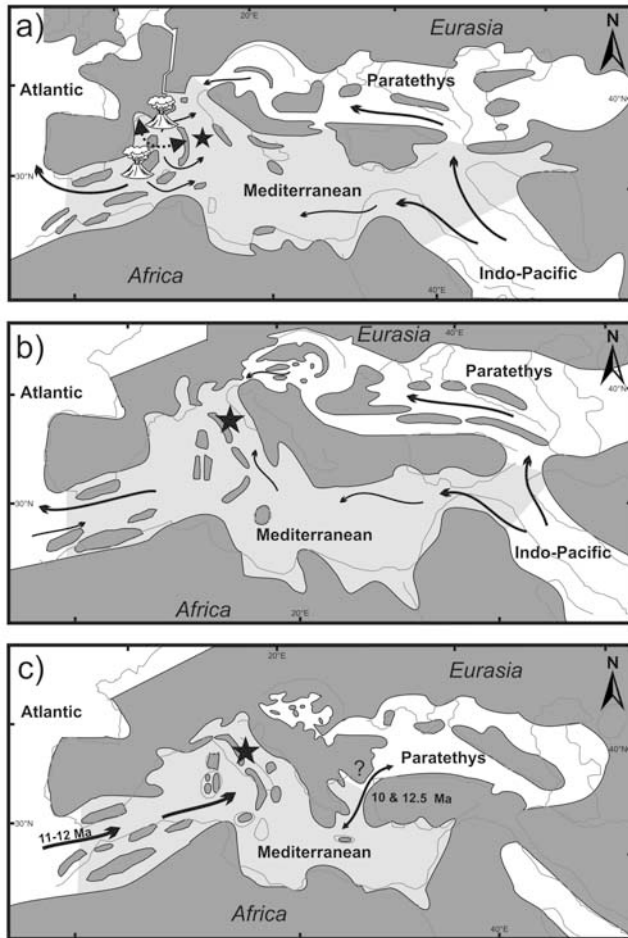


Figure 7. Paleoceanography of the Mediterranean during the Miocene deduced from the isotope data and their paleogeographic interpretation illustrated on the maps of Rögl [1998]. The black star indicates the former position of the UMC samples, and the arrows indicate the seawater currents into the Mediterranean. (a) 25–19 Ma (map: Aquitanian), the period of the opening of the western Mediterranean with active volcanism in the region but an influx of seawater largely from the Indian Ocean. (b) 19–13 Ma (map: Langhian), a dominant local influence on the Mediterranean seawater together with influence through gateways from the Indian Ocean, with an outflow into the Atlantic Ocean. (c) 13–7 Ma (map: Tortonian), alternate influences between the Atlantic and the Paratethys (see text for details).

the paleoclimatic-paleoceanographic evolution of this part of the Mediterranean.

5.6.1. Period From 25 to 19 Ma

[64] This period is characterized by high ϵ_{Nd} values for UMC fossils, two VF samples, also those measured for phosphate beds of Malta [Stille *et al.*, 1996], and foraminifera of the Piedmont basin [Jacobs *et al.*, 1996a]. The values are between those representative of the Indian and Pacific Oceans [Ling *et al.*, 1997; O’Nions *et al.*, 1998] during the Oligo-Miocene and Stille *et al.* [1996] suggested

a direct connection between the Mediterranean and the Pacific Ocean at this time. Some samples from MS, SLO, as well as others from UMC at around 22–24 Ma, and all sampled localities toward the end of this period (19 Ma), have values similar to those of the Indian Ocean (Figure 6). For either a Pacific or an Indian Ocean influence, the same eastern seaway is assumed to have been important [Rögl, 1998]. Furthermore, collision of India with Asia excludes direct inflow from the Pacific Ocean. The Indian Ocean influence in the region is further supported by the ϵ_{Nd} values of the Paratethys (Figure 6a), which were very similar to those of the Indian Ocean at around 19–20 Ma [Kocsis *et al.*, 2008]. Moreover, the older fossils (22–24 Ma) of the northern localities (MS, SLO) might have been influenced by Indian Ocean water, which entered through the Paratethys via the Slovenian corridor into the Mediterranean, which seaway existed during this period [Rögl, 1998].

[65] The siliceous fraction of the sediments in the UMC section, however, also has elevated ϵ_{Nd} values and the low $^{87}\text{Sr}/^{86}\text{Sr}$, supporting important local volcanism in the region that could be linked to the period of opening of the western Mediterranean (see section 5.4). Therefore, instead of a competitive influence between Indian and Pacific water entering into the Mediterranean, strong local volcanism may have influenced the water budget at this time.

5.6.2. Period From 19 to 13 Ma

[66] The seawater Sr isotopic compositions of the Mediterranean sections generally do not correspond to open ocean Miocene values until after ~ 15 Ma (Figure 5c). The low $^{87}\text{Sr}/^{86}\text{Sr}$ of the UMC fossils suggest a local influence with an important contribution of Sr through erosion of Mesozoic carbonates, weathering of which may well have been supported by the subtropical climate during the early depositional phase. In contrast, as these carbonates have low Nd concentrations their contribution of Nd to the seawater budget is probably quite small. The situation is reversed for the Moransengo fossils that record high $^{87}\text{Sr}/^{86}\text{Sr}$ and low $^{143}\text{Nd}/^{144}\text{Nd}$ ratios, indicating erosion of older continental rocks near the southwestern Alps and Apennines [cf. Henry *et al.*, 1997].

[67] The UMC fossils have little differences in their ϵ_{Nd} values during this time, which slowly increases from -9 to -8 . Exceptions to this trend are given by VED-17.2 at 15.3 Ma, with a higher value of -7 and together with analyses from the sediment, suggest another short-lived volcanic influence on the local seawater [Montanari *et al.*, 1994, 1997a, 1997b; Mader *et al.*, 2001]. Another exception is a very negative value down to -10.2 ϵ_{Nd} values at 15.2 Ma (MOR-184). In this case the ϵ_{Nd} value is similar to that of the silicate fraction of the sediment (Figure 6a) and perhaps related to an enhanced weathering of the hinterland together with even more limited water inflow in the area.

[68] Nd isotopic compositions of samples from the Veneto-Friuli area, most of the Moransengo samples, those from the phosphate layers in Malta [Stille *et al.*, 1996], and shark teeth from the Paratethys [Kocsis *et al.*, 2008], all have very similar values to those considered as “background” or average ϵ_{Nd} values of the UMC section (Figure 7). These values are very comparable to a mixed seawater source between Atlantic and Indian Ocean water

(Figure 6). However, fossils of the ODP Site 900 indicate that the eastern Atlantic was not too different in value compared to the Mediterranean during this period, making exact estimates of proportions difficult.

[69] To sum up in agreement with the Sr isotope data, a rather dominant local input together with Indian Ocean influence can be assumed in the Mediterranean at this time, which further have affected the eastern Atlantic as well.

5.6.3. Period From 13 to 8 Ma

[70] The UMC fossils generally recorded normal Miocene open ocean Sr isotopic compositions indicating good connection with the global oceans, whereas the ϵ_{Nd} values fluctuate between the Indian Ocean (13 and 10 Ma) and the Atlantic Ocean (12–11 Ma) compositions (Figures 5 and 6). However, the final cease of the eastern seaway was around 14–13 Ma at the Langhian/Serravallian transition [e.g., Rögl, 1998; Popov *et al.*, 2004] discarding the Indian Ocean originated water in the area. Maybe this closure induced the presence of enhanced Atlantic seawater entering into the Mediterranean shown by the sudden decrease in the ϵ_{Nd} values at 12–11 Ma.

[71] After this period the fossil ϵ_{Nd} values increased again toward the Indian-Ocean-like seawater that marks the diminishing Atlantic effect in the Mediterranean. The Nd budget became controlled by extra inputs either from the local hinterland and/or from the water masses entering from the Paratethys (Figures 6 and 7c). An analogous example for such local water development with similar ϵ_{Nd} values for the Indian Ocean is the modern Mediterranean [Tachikawa *et al.*, 2004]. The Paratethyan connection would be supported by ϵ_{Nd} values at least till 12 Ma (Figure 6a) and it may have lasted longer. Another rather tentative possibility rose up from our ϵ_{Nd} values such as the Indian Ocean reentered into the Mediterranean once again maybe via the Paratethys (~10 Ma), however such statement lacks of support in the view of several other studies [e.g., Rögl and Steininger, 1983; Rögl, 1998; Popov *et al.*, 2004, 2006].

[72] In case of the youngest sample (8.4 Ma) the ϵ_{Nd} value is much lower again, but in this case the $^{87}\text{Sr}/^{86}\text{Sr}$ also deviates from values typical of Miocene open ocean. This might indicate the strengthening of the local influence again in the region together with limited connection toward the open ocean.

[73] At this time interval the gradually cooling climate and the enhanced growth of the East Antarctic ice sheet resulted in a more advanced succession of sea level fall events, which are marked by oxygen isotope maxima (Mi 3 to 6 [cf. Miller *et al.*, 1991]). Unfortunately, our $\delta^{18}\text{O}$ data are not detailed enough to trace unambiguously the Mi events, however isotope record from Sicily yielded these global variations in $\delta^{18}\text{O}$ values for the Mediterranean as well [Turco *et al.*, 2001; Hilgen *et al.*, 2005]. At the transition between the middle and late Miocene (Serravallian/Tortonian), where our lowest ϵ_{Nd} values indicate the presence of Atlantic seawater in the Mediterranean, the record generally show a major sea level fall [Haq *et al.*, 1987; Hardenbol *et al.*, 1998; Miller *et al.*, 1998, 2005] coupled by the Mi5 event [cf. Miller *et al.*, 1991; Westerhold *et al.*, 2005]. On the other hand, before this sea level drop a relatively larger rise occurred [cf. Miller *et al.*, 2005].

[74] Nevertheless, the low ϵ_{Nd} value together with $^{87}\text{Sr}/^{86}\text{Sr}$ ratio that remains typical of the open ocean signifies the enhanced Atlantic influence in the Mediterranean at 12–11 Ma. In the view of the sea level fluctuations, one scenario could be that the Atlantic water inflow may have started by a short sea rise [cf. Miller *et al.*, 2005] but apparently it peaked at a low global sea level [Hardenbol *et al.*, 1998]. After this period the increasing ϵ_{Nd} values show the end of Atlantic dominance which may have been driven by further sea level changes and/or local tectonic adjustment.

6. Conclusion

[75] The Sr, Nd, C, and O isotope compositions of marine fossils and the Sr and Nd isotope compositions of their embedding sediments have been analyzed from sections of the Miocene Mediterranean. Oxygen isotope compositions of benthic and planktonic foraminifera have preserved compositions compatible with their relative habitats and that also vary in concert with those used for evaluating global changes in climate. Carbon isotope compositions also preserved differences characteristic for having equilibrated with the carbon isotope compositions of dissolved inorganic carbon in bottom and surface waters for benthic and planktonic foraminifera, respectively. Furthermore, between 17 to 13 Ma a positive $\delta^{13}\text{C}$ excursion is noted, which correlates well with the globally recognized Monterey carbon isotope event. These results support that the fossils are well preserved and did not experience strong diagenetic overprints.

[76] The radiogenic isotope compositions, measured on the same splits of samples as the stable isotope compositions, when interpreted in conjunction allow for the following paleoceanographic interpretations:

[77] 1. During the period of 25 to 19 Ma the compositions are indicative of the opening of the western Mediterranean and intense volcanism related to major tectonic events. The seawater compositions are locally influenced and do not yet reflect complete open ocean conditions, even though the gateway to the Indian Ocean was already of importance.

[78] 2. During the period between 19 and 13 Ma the influence of seawater from the Indian Ocean strengthened, also affecting the Atlantic Ocean at the Mediterranean outflow. However, the $^{87}\text{Sr}/^{86}\text{Sr}$ of the fossils do not yet reflect Miocene open ocean conditions for the northern Mediterranean basins (at least till 15 Ma), suggestive of strong tectonic activity in the Alps with a predominant Sr input from weathering of Mesozoic carbonates but also significant erosion of older crustal rocks near the Alps. A warm subtropical climate suggested by the oxygen isotopic compositions favored intense weathering. Brief excursions most notably in the Nd isotopic compositions may indicate sporadic volcanic events.

[79] 3. Between 13 and 10 Ma the Sr isotope record supports open ocean conditions, while the Nd isotope record suggests a fluctuating influence of Atlantic versus Paratethys and/or locally evolved seawater in the Mediterranean, which was driven by global sea level changes and by local tectonic adjustments.

[80] **Acknowledgments.** We thank the Ocean Drilling Program for providing the core samples of ODP Site 900 and Thomas Mühlstarrer for donating his samples from the Moransengo area. This research was generously funded by the Swiss National Science Foundation (SNF 200021-100530). We also appreciate the kind help of David Haig (UWA)

for the revision of the micropaleontological information. Discussions with and comments by Peter Baumgartner greatly aided our interpretation. The comprehensive reviews by R. Mark Leckie and an anonymous reviewer are much appreciated and have also helped to improve the manuscript.

References

- Abouchami, W., S. J. G. Galer, and A. Koschinsky (1999), Pb and Nd isotopes in NE Atlantic Fe-Mn crusts: Proxies for trace metal paleosources and paleocean circulation, *Geochim. Cosmochim. Acta*, **63**, 1489–1505, doi:10.1016/S0016-7037(99)00068-X.
- Albarède, F., and S. L. Goldstein (1992), A world map of Nd isotopes in seafloor ferromanganese deposits, *Geology*, **20**, 761–763, doi:10.1130/0091-7613(1992)020<0761:WMONII>2.3.CO;2.
- Albarède, F., S. L. Goldstein, and D. Dautel (1997), The $^{143}\text{Nd}/^{144}\text{Nd}$ of Mn nodules from the Southern and Indian oceans, the global oceanic Nd budget, and their bearing on the deep ocean circulation during the Quaternary, *Geochim. Cosmochim. Acta*, **61**, 1277–1291, doi:10.1016/S0016-7037(96)00404-8.
- Balogh, K., M. Delle Rose, F. Guerrera, L. Ravasz-Baranyai, and F. Veneri (1993), New data concerning the inframiocenic ‘Biscario volcanoclastic event’ (Umbrio-Marche Apennines) and comparison with similar occurrences, *G. Geol.*, **55**, 83–104.
- Beccaluva, L., G. Bianchini, and F. Siena (2004), Tertiary-Quaternary volcanism and tectonomagmatic evolution in Italy, in *Geology of Italy, Special Volume of the Italian Geological Society for the IGC 32 Florence*, edited by U. Crescenti et al., pp. 153–160, Soc. Geol. It., Rome.
- Bertram, C. J., and H. Elderfield (1993), The geochemical balance of the rare earth elements and Nd isotopes in the oceans, *Geochim. Cosmochim. Acta*, **57**, 1957–1986, doi:10.1016/0016-7037(93)90087-D.
- Boyle, E. A. (1981), Cadmium, zinc, copper, and barium in foraminifera tests, *Earth Planet. Sci. Lett.*, **53**, 11–35, doi:10.1016/0012-821X(81)90022-4.
- Brügel, A., I. Dunkl, W. Frisch, J. Kuhlmann, and K. Balogh (2000), The record of Periadriatic volcanism in the Eastern Alpine Molasse zone and its paleogeographic implications, *Terra Nova*, **12**, 42–47, doi:10.1046/j.1365-3121.2000.00269.x.
- Bryant, J. D., D. S. Jones, and P. A. Mueller (1995), Influence of freshwater flux on $^{87}\text{Sr}/^{86}\text{Sr}$ chronostratigraphy in marginal marine environments and dating of vertebrate and invertebrate faunas, *J. Paleontol.*, **69**, 1–6.
- Burke, W. H., R. E. Denison, E. A. Hetherington, R. B. Koepnick, H. F. Nelson, and J. B. Otto (1982), Variation of seawater $^{87}\text{Sr}/^{86}\text{Sr}$ throughout Phanerozoic time, *Geology*, **10**, 516–519, doi:10.1130/0091-7613(1982)10<516:VOSSTP>2.0.CO;2.
- Burton, K. W., and D. Vance (2000), Glacial-interglacial variations in the neodymium isotope composition of seawater in the Bay of Bengal recorded by planktonic foraminifera, *Earth Planet. Sci. Lett.*, **176**, 425–441, doi:10.1016/S0012-821X(00)00111-X.
- Burton, K. W., H.-F. Ling, and R. K. O’Nions (1997), Closure of the Central American Isthmus and its effect on deep-water formation in the North Atlantic, *Nature*, **386**, 382–385, doi:10.1038/386382a0.
- Burton, K. W., D.-C. Lee, J. N. Christensen, A. N. Halliday, and J. R. Hein (1999), Actual timing of neodymium isotopic variations recorded by Fe-Mn crusts in the western North Atlantic, *Earth Planet. Sci. Lett.*, **171**, 149–156, doi:10.1016/S0012-821X(99)00138-7.
- Clari, P., F. Dela Pierre, A. Novaretti, and M. Timpanelli (1995), Late Oligocene-Miocene sedimentary evolution of the critical Alps/Apennines junction: The Monferrato area, northwestern Italy, *Terra Nova*, **7**, 144–152, doi:10.1111/j.1365-3121.1995.tb00683.x.
- Cleaveland, L. C., J. Jensen, S. Goese, D. M. Bice, and A. Montanari (2002), Cyclostratigraphic analysis of pelagic carbonates at Monte dei Corvi (Ancona, Italy) and astronomical correlation of the Serravallian-Tortonian boundary, *Geology*, **30**, 931–934, doi:10.1130/0091-7613(2002)030<0931:CAOPCA>2.0.CO;2.
- Deino, A., et al. (1997), Integrated stratigraphy of the upper Burdigalian-lower Langhian section at Moria (Marche region, Italy), in *Miocene Stratigraphy: An Integrated Approach*, *Dev. in Palaeontol. and Stratigr.*, vol. 15, edited by A. Montanari, G. S. Odin, and R. Coccioni, pp. 315–341, Elsevier, Amsterdam.
- de Kaenel, E., and G. Villa (1996), Oligocene-Miocene calcareous nannofossils from the Iberia Abyssal Plain, *Proc. Ocean Drill. Program Sci. Results*, **149**, 79–145.
- DePaolo, D. J. (1986), Detailed record of the Neogene Sr isotopic evolution of seawater from DSDP site 590B, *Geology*, **14**, 103–106, doi:10.1130/0091-7613(1986)14<103:DROTNS>2.0.CO;2.
- DePaolo, D. J., and B. L. Ingram (1985), High-resolution stratigraphy with strontium isotopes, *Science*, **227**, 938–941, doi:10.1126/science.227.4689.938.
- Douglas, R. G., and S. M. Savin (1975), Oxygen and carbon isotope analyses of Cretaceous and Tertiary foraminifera from Shatsky Rise and other sites in the North Pacific Ocean, *Initial Rep. Deep Sea Drill. Proj.*, **32**, 509–520.
- Douglas, R. G., and S. M. Savin (1978), Oxygen isotopic evidence for the depth stratification of Tertiary and Cretaceous planktonic foraminifera, *Mar. Micropaleontol.*, **3**, 175–196, doi:10.1016/0377-8398(78)90004-X.
- Faure, G. (1986), *Principles of Isotope Geology*, 2nd ed., 589 pp., John Wiley, New York.
- Fodor, L., B. Jelen, E. Márton, D. Skabeme, J. Car, and M. Vrabec (1998), Miocene-Pliocene tectonic evolution of the Slovenian Periadriatic Line: Implication for Alpine-Carpathian extrusion models, *Tectonics*, **17**, 690–709, doi:10.1029/98TC01605.
- Frank, M. (2002), Radiogenic isotopes. Tracers of past ocean circulation and erosional input, *Rev. Geophys.*, **40**(1), 1001, doi:10.1029/2000RG000094.
- Frank, M., B. C. Reynolds, and R. K. O’Nions (1999), Nd and Pb isotopes in Atlantic and Pacific water masses before and after closure of the Panama gateway, *Geology*, **27**, 1147–1150, doi:10.1130/0091-7613(1999)027<1147:NA-PIIA>2.3.CO;2.
- Frank, M., N. Whiteley, S. Kasten, J. R. Hein, and R. K. O’Nions (2002), North Atlantic Deep Water export to the Southern Ocean over the past 14 Myr: Evidence from Nd and Pb isotopes in ferromanganese crusts, *Paleoceanography*, **17**(2), 1022, doi:10.1029/2000PA000606.
- Gervais, E. (1996), Cretaceous to Quaternary planktonic foraminiferal biostratigraphy of the Iberia Abyssal Plain, *Proc. Ocean Drill. Program Sci. Results*, **149**, 165–192.
- Gradstein, F. M., J. G. Ogg, and A. Smith (Eds.) (2004), *A Geologic Time Scale 2004*, Cambridge Univ. Press, Cambridge, U.K.
- Gueguen, E., C. Doglioni, and M. Fernandez (1998), On the post-25 Ma geodynamic evolution of the western Mediterranean, *Tectonophysics*, **298**, 259–269, doi:10.1016/S0040-1951(98)00189-9.
- Gutjahr, M., M. Frank, C. H. Stirling, V. Klemm, T. van de Fliedert, and A. N. Halliday (2007), Reliable extraction of a deepwater trace metal isotope signal from Fe-Mn oxyhydroxide coatings of marine sediments, *Chem. Geol.*, **242**, 351–370, doi:10.1016/j.chemgeol.2007.03.021.
- Hagmaier, M. (2002), Isotopie (C, O und Sr) von Foraminiferen der zentralen nördlichen Paratethys (Bayerische Molasse, Wiener Becken) im Miozän als paläozeanographische Proxies, diploma thesis, pp. 1–69, Univ. of Tübingen, Tübingen, Germany.
- Haq, B. U., J. Hardenbol, and P. R. Vail (1987), Chronology of fluctuating sea levels since the Triassic (250 million years ago to present), *Science*, **235**, 1156–1167, doi:10.1126/science.235.4793.1156.
- Hardenbol, J., J. Thierry, M. B. Farley, T. H. Jaquin, and P. R. Vail (1998), Mesozoic and Cenozoic sequence chronostratigraphic framework of European basins, *Spec. Publ. SEPM Soc. Sediment. Geol.*, **60**, 1–13.
- Hegner, E., H. J. Walter, and M. Satir (1995), Pb-Sr-Nd isotopic compositions and trace element geochemistry of megacrysts and melilitites from the Tertiary Urach volcanic field: Source compositions of small volume melts under SW Germany, *Contrib. Mineral. Petrol.*, **122**, 322–335, doi:10.1007/s004100050131.
- Henry, P., E. Deloule, and A. Michard (1997), The erosion of the Alps: Nd isotopic and geochemical constraints on the sources of the peri-Alpine Molasse sediments, *Earth Planet. Sci. Lett.*, **146**, 627–644, doi:10.1016/S0012-821X(96)00252-X.
- Hilgen, F. J., H. Abdul Aziz, W. Krijgsman, I. Raffi, and E. Turco (2003), Integrated stratigraphy and astronomical tuning of the Serravallian and lower Tortonian at Monte dei Corvi (Middle-Upper Miocene, northern Italy), *Paleogeogr. Palaeoclimatol. Palaeoecol.*, **199**, 229–264, doi:10.1016/S0031-0182(03)00505-4.
- Hilgen, F. J., H. Abdul Aziz, D. Bice, S. Iaccarino, W. Krijgsman, K. Kuiper, A. Montanari, I. Raffi, E. Turco, and W.-J. Zachariasse (2005), The global boundary Stratotype Section and Point (GSSP) of the Tortonian Stage (Upper Miocene) at Monte Dei Corvi, *Episodes*, **28**, 6–17.

- Hodell, D. L., P. A. Mueller, and J. R. Garrido (1991), Variations in the strontium isotopic composition of seawater during the Neogene, *Geology*, *19*, 24–27, doi:10.1130/0091-7613(1991)019<0024:VITSIC>2.3.CO;2.
- Jacobs, E., M. Steinmann, P. M. Biolzi, and P. Stille (1996a), Sr isotope stratigraphy and variations in Nd isotopic composition of foraminifera from Lemme-Carrosio section (northern Italy), *G. Geol.*, *58*, 111–117.
- Jacobs, E., H. Weissert, G. Shields, and P. Stille (1996b), The Monterey event in the Mediterranean: A record from shelf sediments of Malta, *Paleoceanography*, *11*, 717–728, doi:10.1029/96PA02230.
- Jacobsen, S. B., and G. J. Wasserburg (1980), Sm-Nd isotopic evolution of chondrites, *Earth Planet. Sci. Lett.*, *50*, 139–155, doi:10.1016/0012-821X(80)90125-9.
- Jeandel, C., T. Arsouze, F. Lacan, P. Téchiné, and J.-C. Dutay (2007), Isotopic Nd compositions and concentrations of the lithogenic inputs into the ocean: A compilation, with an emphasis on the margins, *Chem. Geol.*, *239*, 156–164, doi:10.1016/j.chemgeo.2006.11.013.
- Jelen, B., and H. Rifej (2002), Stratigraphic structure of the B1 Tertiary tectonostratigraphic unit in eastern Slovenia, *Geologija*, *45*, 115–138.
- Jovane, L., F. Florindo, R. Coccioni, J. Dinarès-Turell, A. Marsili, S. Monechi, A. P. Roberts, and M. Sprovieri (2007), The middle Eocene climatic optimum event in the Contessa Highway section, Umbrian Apennines, Italy, *Geol. Soc. Am. Bull.*, *119*, 413–427, doi:10.1130/B25917.1.
- Kocsis, L., T. W. Vennemann, and D. Fontignie (2007), Migration of sharks into freshwater systems during the Miocene and implications for Alpine paleoelevation, *Geology*, *35*, 451–454, doi:10.1130/G23404A.1.
- Kocsis, L., T. W. Vennemann, E. Hegner, D. Fontignie, and T. Tütken (2008), Constraints on Miocene oceanography and climate in the Western and Central Paratethys: O-, Sr-, and Nd-isotope compositions of marine fish and mammal remains, *Palaeogeogr. Palaeoclimatol. Palaeoecol.*, in press.
- Koepnick, R. B., W. H. Burke, R. E. Denison, E. A. Hetherington, H. F. Nelson, J. B. Otto, and L. E. Waite (1985), Construction of the seawater ⁸⁷Sr/⁸⁶Sr curve for the Cenozoic and Cretaceous: Supporting data, *Chem. Geol.*, *58*, 55–81, doi:10.1016/0009-2541(85)90179-2.
- Kroopnick, P. (1985), The distribution of ¹³C of δCO₂ in the world oceans, *Deep Sea Res., Part A*, *32*, 57–84, doi:10.1016/0198-0149(85)90017-2.
- Kuhlemann, J., W. Frisch, I. Dunkl, and B. Székely (2001), Quantifying tectonic versus erosive denudation by the sediment budget: The Miocene core complexes of the Alps, *Tectonophysics*, *330*, 1–23, doi:10.1016/S0040-1951(00)00209-2.
- Lacan, F., and C. Jeandel (2005), Neodymium isotopes as a new tool for quantifying exchange fluxes at the continent-ocean interface, *Earth Planet. Sci. Lett.*, *232*, 245–257, doi:10.1016/j.epsl.2005.01.004.
- Ling, H.-F., K. W. Burton, R. K. O’Nions, B. S. Kamber, F. von Blanckenburg, A. J. Gibb, and J. R. Hein (1997), Evolution of Nd and Pb isotopes in central Pacific seawater from ferromanganese crusts, *Earth Planet. Sci. Lett.*, *146*, 1–12, doi:10.1016/S0012-821X(96)00224-5.
- Mader, D., A. Montanari, J. Gattacocca, C. Koeberl, R. Handler, and R. Coccioni (2001), ⁴⁰Ar/³⁹Ar dating of a Langhian biotite-rich clay layer in the pelagic sequence of the Cònero Riviera, Ancona, Italy, *Earth Planet. Sci. Lett.*, *194*, 111–126, doi:10.1016/S0012-821X(01)00544-1.
- Mahlen, N. J., C. M. Johnson, L. P. Baumgartner, and B. L. Beard (2005), Provenance of Jurassic Tethyan sediments in the HP/UHP Zermatt-Saas ophiolite, western Alps, *Geol. Soc. Am. Bull.*, *117*, 530–544, doi:10.1130/B25545.1.
- Martin, E. E., and B. A. Haley (2000), Fossil fish teeth as proxies for seawater Sr and Nd isotopes, *Geochim. Cosmochim. Acta*, *64*, 835–847, doi:10.1016/S0016-7037(99)00376-2.
- Massari, F., P. Grandesso, C. Stefani, and P. G. Jobstraibizer (1986), A small polyhistory foreland basin evolving in a context of oblique convergence: The Venetian basin (Chattian to Recent, Southern Alps, Italy), in *Foreland Basins*, edited by P. A. Allen and P. Homewood, *Spec. Publ. Int. Assoc. Sedimentol.*, *8*, 141–168.
- McArthur, J. M., R. J. Howarth, and T. R. Bailey (2001), Strontium isotope stratigraphy: LOW-ESS version 3: Best fit to the marine Sr-isotope curve for 0–509 Ma and accompanying look-up table for deriving numerical age, *J. Geol.*, *109*, 155–170, doi:10.1086/319243.
- Milkert, D., B. Alonso, L. Liu, X. Zhao, M. Comas, and E. de Kaenel (1996), Sedimentary facies and depositional history of the Iberia Abyssal Plain, *Proc. Ocean Drill. Program Sci. Results*, *149*, 685–704.
- Miller, K. G., R. G. Fairbanks, and G. S. Mountain (1987), Tertiary oxygen isotope synthesis, sea level history and continental margin erosion, *Paleoceanography*, *2*, 1–19, doi:10.1029/PA0021001p00001.
- Miller, K. G., M. D. Feigenson, J. D. Wright, and B. M. Clement (1991), Miocene isotope reference section, Deep Sea Drilling Project Site 608: An evaluation of isotope and biostratigraphic resolution, *Paleoceanography*, *6*, 33–52, doi:10.1029/90PA01941.
- Miller, K. G., G. S. Mountain, J. V. Browning, M. Kominz, P. J. Sugarman, N. Christie-Blick, and M. E. Katz (1998), Cenozoic global sea level, sequences, and the New Jersey transect: Results from coastal plain and continental slope drilling, *Rev. Geophys.*, *36*, 569–601, doi:10.1029/98RG01624.
- Miller, K. G., M. A. Kominz, J. V. Browning, J. D. Wright, G. S. Mountain, M. E. Katz, P. J. Sugarman, B. S. Cramer, N. Christie-Blick, and S. F. Pekar (2005), The Phanerozoic record of global sea-level change, *Science*, *310*, 1293–1298, doi:10.1126/science.1116412.
- Montanari, A., S. Carey, R. Coccioni, and A. Deino (1994), Sardinian provenance for Lower Miocene tephra in the pelagic sequence of the northeastern Apennines, *Tectonics*, *13*, 1120–1134, doi:10.1029/94TC00295.
- Montanari, A., D. M. Bice, R. Capo, R. Coccioni, A. Deino, D. J. DePaolo, L. Emmanuel, S. Monechi, M. Renard, and D. Zevenboom (1997a), Integrated stratigraphy of the Chattian to mid-Burdigalian pelagic sequence of the Contessa Valley (Gubbio, Italy), in *Miocene Stratigraphy: An Integrated Approach*, *Dev. in Palaeontol. and Stratigr.*, vol. 15, edited by A. Montanari, G. S. Odin, and R. Coccioni, pp. 249–277, Elsevier, Amsterdam.
- Montanari, A., et al. (1997b), Integrated stratigraphy of the Middle and Upper Miocene pelagic sequence of the Cònero Riviera (Marche region, Italy), in *Miocene Stratigraphy: An Integrated Approach*, *Dev. in Palaeontol. and Stratigr.*, vol. 15, edited by A. Montanari, G. S. Odin,
- and R. Coccioni, pp. 409–450, Elsevier, Amsterdam.
- Mühlstrasser, T. (2002), Paleoceanographic history of the northwestern Tethyan realm for the Late Oligocene through Middle Miocene, *Tübinger Mikropalaontol. Mitt.*, *24*, 1–119.
- O’Nions, R. K., M. Frank, F. von Blanckenburg, and H.-F. Ling (1998), Secular variation of Nd and Pb isotopes in ferromanganese crusts from the Atlantic, Indian and Pacific Oceans, *Earth Planet. Sci. Lett.*, *155*, 15–28, doi:10.1016/S0012-821X(97)00207-0.
- Orszag-Sperber, F. (2006), Changing perspectives in the concept of “Lago-Mare” in Mediterranean Late Miocene evolution, *Sediment. Geol.*, *188–189*, 259–277, doi:10.1016/j.sedgeo.2006.03.008.
- Palmer, M. R. (1985), Rare earth elements in foraminifera test, *Earth Planet. Sci. Lett.*, *73*, 285–298, doi:10.1016/0012-821X(85)90077-9.
- Palmer, M. R., and H. Elderfield (1985), Variations in the Nd isotopic composition of foraminifera from Atlantic Ocean sediments, *Earth Planet. Sci. Lett.*, *73*, 299–305, doi:10.1016/0012-821X(85)90078-0.
- Palmer, M. R., and H. Elderfield (1986), Rare earth elements and neodymium isotopes in ferromanganese oxide coatings of Cenozoic foraminifera from Atlantic Ocean, *Geochim. Cosmochim. Acta*, *50*, 409–417, doi:10.1016/0016-7037(86)90194-8.
- Piana, F., and R. Polino (1995), Tertiary structural relationships between Alps and Apennines: The critical Torino Hill and Monferrato area, northwestern Italy, *Terra Nova*, *7*, 138–143, doi:10.1111/j.1365-3121.1995.tb00682.x.
- Pieprgras, D. J., and G. J. Wasserburg (1980), Neodymium isotopic variations in seawater, *Earth Planet. Sci. Lett.*, *50*, 128–138, doi:10.1016/0012-821X(80)90124-7.
- Pomiès, C., G. R. Davies, and M.-H. S. Conan (2002), Neodymium in modern foraminifera from the Indian Ocean: Implications for the use of foraminiferal Nd isotope compositions in paleo-oceanography, *Earth Planet. Sci. Lett.*, *203*, 1031–1045, doi:10.1016/S0012-821X(02)00924-X.
- Popov, S. V., F. Rögl, A. Y. Rozanov, F. F. Steininger, I. G. Shcherba, and M. Kovac (2004), Lithological-Paleogeographic maps of Paratethys, 10 maps Late Eocene to Pliocene, *Cour. Forschungsinst. Senckenberg*, *250*, 1–46.
- Popov, S. V., I. G. Shcherba, L. B. Ilyina, L. A. Nevesskaya, N. P. Paramonova, S. O. Khondkarian, and I. Magyar (2006), Late Miocene to Pliocene palaeogeography of the Paratethys and its relation to the Mediterranean, *Palaeogeogr. Palaeoclimatol. Palaeoecol.*, *238*, 91–106, doi:10.1016/j.palaeo.2006.03.020.
- Reynolds, B. C., M. Frank, and R. K. O’Nions (1999), Nd- and Pb-isotope time series from Atlantic ferromanganese crusts: Implications for changes in provenance and paleocirculation over the last 8 Myr, *Earth Planet. Sci. Lett.*, *173*, 381–396, doi:10.1016/S0012-821X(99)00243-5.
- Rögl, F. (1998), Palaeogeographic considerations for the Mediterranean and Paratethys Seaways (Oligocene to Miocene), *Ann. Naturhist. Mus. Wien, Ser. A*, *99*, 279–310.
- Rögl, F., and F. F. Steininger (1983), Vom Zerfall der Tethys zu Mediterran und Paratethys. Die neogene Paläogeographie und Paläinastik des zirkum-mediterranen Raumes, *Ann. Naturhist. Mus. Wien, Ser. A*, *84*, 135–163.
- Rosenbaum, G., G. S. Lister, and C. Duboz (2002), Reconstruction of the tectonic evolution of the western Mediterranean since the

- Oligocene, in *Reconstruction of the Evolution of the Alpine-Himalayan Orogen*, edited by G. Rosenbaum and G. S. Lister, *J. Virtual Explorer*, 8, 107–130.
- Savin, S., L. Abel, H. Barrera, D. Hodell, G. Keller, J. P. Kennett, J. Killingley, M. Murphy, and E. Vincent (1985), The evolution of Miocene surface and near-surface marine temperatures: Oxygen isotope evidence, in *The Miocene Ocean*, edited by J. P. Kennett, *Mem. Geol. Soc. Am.*, 163, 49–82.
- Scher, H. D., and E. E. Martin (2006), Timing and climatic consequences of the opening of Drake Passage, *Science*, 312, 428–430, doi:10.1126/science.1120044.
- Spötl, C., and T. W. Vennemann (2003), Continuous-flow IRMS analysis of carbonate minerals, *Rapid Commun. Mass Spectrom.*, 17, 1004–1006, doi:10.1002/rcm.1010.
- Staudigel, H., P. Doyle, and A. Zindler (1985), Sr and Nd isotope systematics in fish teeth, *Earth Planet. Sci. Lett.*, 76, 45–56, doi:10.1016/0012-821X(85)90147-5.
- Stille, P., M. Steinmann, and R. S. Riggs (1996), Nd isotope evidence for the evolution of the paleocurrents in the Atlantic and Tethys Oceans during the past 180 Ma, *Earth Planet. Sci. Lett.*, 144, 9–19, doi:10.1016/0012-821X(96)00157-4.
- Tachikawa, K., C. Jeandel, and M. Roy-Barman (1999), A new approach to the Nd residence time in the ocean: The role of atmospheric inputs, *Earth Planet. Sci. Lett.*, 170, 433–446, doi:10.1016/S0012-821X(99)00127-2.
- Tachikawa, K., M. Roy-Barman, A. Michard, D. Thouren, D. Yeghicheyan, and C. Jeandel (2004), Neodymium isotopes in the Mediterranean Sea: Comparison between seawater and sediment signals, *Geochim. Cosmochim. Acta*, 68(14), 3095–3106, doi:10.1016/j.gca.2004.01.024.
- Turco, E., F. J. Hilgen, L. J. Lourens, N. J. Shackleton, and W. J. Zachariasse (2001), Punctuated evolution of global climate cooling during the late Middle to early Late Miocene: High-resolution planktonic foraminiferal and oxygen isotope records from the Mediterranean, *Paleoceanography*, 16, 405–423, doi:10.1029/2000PA000509.
- Vance, D., and K. Burton (1999), Neodymium isotopes in planktonic foraminifera: A record of the response of continental weathering and ocean circulation rates to climate change, *Earth Planet. Sci. Lett.*, 173, 365–379, doi:10.1016/S0012-821X(99)00244-7.
- Vance, D., A. E. Scrivner, P. Beney, M. Staubwasser, G. M. Henderson, and N. C. Slowey (2004), The use of foraminifera as a record of the past neodymium isotope composition of seawater, *Paleoceanography*, 19, PA2009, doi:10.1029/2003PA000957.
- Veizer, J. (1989), Strontium isotopes in seawater through time, *Annu. Rev. Earth Planet. Sci.*, 17, 141–167, doi:10.1146/annurev.ea.17.050189.001041.
- Vennemann, T. W., and E. Hegner (1998), Oxygen, strontium and neodymium isotope composition of shark teeth as a proxy for the palaeoceanography and palaeoclimatology of the Miocene northern Alpine Paratethys, *Palaeogeogr. Palaeoclimatol. Palaeoecol.*, 142, 107–121, doi:10.1016/S0031-0182(98)00062-5.
- Weldeab, S., K.-C. Emeis, C. Hemleben, T. W. Vennemann, and H. Schultz (2002), Sr and Nd isotope composition of Late Pleistocene sapropels and nonsapropelic sediments from Eastern Mediterranean Sea: Implications for detrital influx and climatic conditions in the source areas, *Geochim. Cosmochim. Acta*, 66, 3585–3598, doi:10.1016/S0016-7037(02)00954-7.
- Westerhold, T., T. Bickert, and U. Röhl (2005), Middle to late Miocene oxygen isotope stratigraphy of ODP site 1085 (SE Atlantic): New constraints on Miocene climate variability and sea-level fluctuations, *Palaeogeogr. Palaeoclimatol. Palaeoecol.*, 217, 205–222, doi:10.1016/j.palaeo.2004.12.001.
- Zachos, J., M. Pagani, L. Sloan, E. Thomas, and K. Billups (2001), Trends, rhythms, and aberrations in global climate 65 Ma to present, *Science*, 292, 686–693, doi:10.1126/science.1059412.

C. Baumgartner, Institut de Géologie et Paléontologie, University of Lausanne, UNIL–Anthropole, CH-1015 Lausanne, Switzerland.

D. Fontignie, Section des Sciences de la Terre, Département de Minéralogie, University of Geneva, CH-1205 Geneva, Switzerland.

B. Jelen, Geological Survey of Slovenia, 1000 Ljubljana, Slovenia.

L. Kocsis and T. W. Vennemann, Institut de Minéralogie et Géochimie, University of Lausanne, UNIL–Anthropole, CH-1015 Lausanne, Switzerland. (laszlo.kocsis@unil.ch)

A. Montanari, Osservatorio Geologico di Coldigioco, I-62020 Frontale di Apiro, Italy.